Dynamics of a slowly-varying sand bed in a circular pipe

Laurence Girolami, John D. Sherwood, François Charru

Dynamics of a slowly-varying sand bed in a circular pipe

L. Girolami [a,1], J.D. Sherwood [b,*], F. Charru [a]

[a] IMFT, Université de Toulouse CNRS-INPT-UPS, F31400 Toulouse, France
[b] DAMTP, University of Cambridge, Wilberforce Road, Cambridge CB3 0WA, UK

Keywords:
Pipe flow
Sand bed
Secondary flow
Stability

A B S T R A C T

The long wave-length dynamics and stability of a bed of sand occupying the lower segment of a circular pipe are studied analytically up to first-order in the small parameter characterizing the slope of the bed. The bed is assumed to be at rest, with at most a thin sand layer (the bedload) moving at the sheared interface. When the sand bed is plane, with depth independent of position z along the axis of the pipe, the velocity of the liquid is known from previous studies of stratified laminar flow of two Newtonian liquids (the lower one with infinite viscosity representing the sand bed). When the depth of the sand bed varies with z, secondary flows develop in the cross-sectional (x, y) plane, and these are computed numerically, assuming that the sand bed remains a straight horizontal line in the cross-sectional plane. The mean shear stress acting on the perturbed sand bed is then determined both from the computed secondary flows and by means of the averaged equations of Luchini and Charru. The latter approach requires knowledge only of the flow over the unperturbed, flat sand bed, combined with an accurate approximation of the distribution of the perturbed stresses between the pipe wall and the sand bed. The perturbed stresses determined by the two methods agree well with each other. Using these stresses, it is then possible to apply standard theories of bed stability to determine the balance between the destabilizing effect of inertial (out-of-phase) stresses and the stabilizing effects of gravity and relaxation of the particle flux, and various examples are considered.

1. Introduction

The transport of sand/water slurries along a horizontal pipeline is of commercial importance, and has therefore been the subject of many studies, reviewed by e.g., Peker and Helvacı (2008); Goharzadeh et al. (2013); and Soepyan et al. (2014). The prediction and control of transport (or settling) of entrained sand in petroleum pipelines is similarly important (Salama, 2000).

At high fluid velocities the particles are suspended and flow with the fluid. However, at low velocities the particles (if denser than the fluid) sediment under gravity, and a stationary bed of particles forms on the lower side of the pipe (Turian et al., 1987). Our interest here lies in the regime of moderate fluid shear stress on the bed, when particles at the bed surface are slowly entrained into a thin moving layer (e.g., Oroskar and Turian, 1980; Takahashi and Masuyama, 1991; Doron and Barnea, 1995, 1996; Turian et al., 1987; Peysson et al., 2009). This moving layer (the bedload layer) has a thickness of just a few particle diameters.

Many studies have concentrated on the flow rates of the sand and water as functions of the applied pressure gradient (e.g., Doron et al., 1987; Kuru et al., 1995; Ouriemi et al., 2009a). However, a crucial issue for bedload transport is the shear stress exerted by the fluid flow over the bed: this stress determines the particle flow rate. The upper surface of the bed is usually wavy (rather than plane), so that the shear stress and particle flow rate are non-uniform in the streamwise direction, leading to the propagation of a complex pattern of sand waves, see e.g., the review by Charru et al. (2013). These waves are of both scientific and engineering interest: ripples and dunes are known to have strong consequences on flow rates and pressure gradients (Takahashi et al., 1989; Takahashi and Masuyama, 1991; Ouriemi et al., 2009b; Al-Lababidi et al., 2012).

The aim of this paper is to provide a set of area-averaged equations governing slow variations of the fluid flow and sand bed, consistent up to first-order in the small-slope parameter. We then use these equations to analyze the linear stability of the bed. The analysis is restricted to laminar flow, with the usual quasistatic assumption that the time scale for bed height variations is long compared to the hydrodynamic time scale, so that the flow may be calculated as if the bed profile were fixed.

* Corresponding author. Tel.: +44 1223760436.
[1] Present address: GéHCO, Université François Rabelais de Tours, Campus Grandmont, 37200 Tours, France
E-mail address: jds60@cam.ac.uk (J.D. Sherwood).

We first (Section 2) discuss the velocity profile and shear stresses in fluid flowing through a pipe in which the sand bed is uniform along the length of the pipe. When the height of the sand bed varies slowly in the axial direction, not only is there a slow variation in the axial velocity of fluid along the pipe, but secondary flows are set up in the cross-section. Such flows are discussed in Section 3. In Section 4 we review a standard theory for the movement of sand grains at the bed surface due to the hydrodynamic bed stress. In Section 5 we derive the set of area-averaged equations for the fluid flow rate, particle flow rate and bed height, assuming that the sand flux is a function of the mean stress averaged over the width of the bed (the detailed stress distribution is ignored). The equations are based on the analysis of Luchini and Charru (2010a) of slowly-varying laminar flows which appeals to the stationarity of the viscous dissipation term in the energy equation, combined with the approximation that the ratio of the shear force acting on the bed to the shear force acting on the wetted wall of the pipe is the same at first-order as at zeroth-order. These equations, although consistent up to the first-order in the small-slope parameter, require only the parallel-flow analytical results (*i.e.,* they do not require the calculation of the first-order flow disturbance over the slowly-varying sand bed). The validity of this analysis is confirmed by comparison with the full first-order numerical results presented in Section 3. As an illustration of the use of the area-integrated equations, a stability analysis of the plane bed is performed in Section 6.

The analysis is restricted to Newtonian fluids, and therefore is inappropriate for either concentrated slurries of particles or for non-Newtonian crude petroleum: however, it is a useful starting point even for such for fluids. The Reynolds number will be required to be sufficiently low for the basic flow within the pipe to be laminar, but, as is standard in long wavelength analysis of nearly parallel flow, the Reynolds number need not be small compared to unity (as will be discussed in Section 3). The regime that we shall investigate is that in which particles at the surface of the sand bed are just starting to move due to the stress imposed on them by the fluid flowing above them in the pipe. Thus the analysis applies to a restricted range of flow rates which is, nevertheless, an important one, since it separates the regime in which the bed is at rest (growing slowly if further particles are deposited) from that in which the particle bed starts to be eroded (as would be required for cleaning out the pipe). We shall re-visit these restrictions in Section 7, where they can be made explicit in terms of the analysis of Sections 2–6.

2. Liquid flow through a pipe with a uniform sand bed

The geometry that we consider is shown in Fig. 1. The pipe has radius R. A bed of sand at the base of the pipe subtends an angle $2\delta_b$ at the center of the pipe, and has a plane, horizontal upper surface AEC. The upper part of the pipe is occupied by liquid, and the portion of the circular pipe wall that is wetted by liquid subtends an angle $2\delta_w = 2(\pi - \delta_b)$ at the center of the pipe.

We set up Cartesian coordinates, with z axis parallel to the axis of the pipe and with (x, y) in the cross-sectional plane of the pipe. The y axis is vertical, along the symmetry axis, and the x axis is horizontal, joining the two triple points A and C where liquid, the pipe wall and the sand bed meet (Fig. 1). We assume that the interface between the sand bed and the liquid is plane, and that it coincides with the x axis $y = 0$. We shall occasionally use cylindrical polar coordinates (r, ψ, z), with $\psi = 0$ directed along the y axis.

The cross-sectional area A of the portion of pipe occupied by liquid can be found by elementary methods, and is

$$A = R^2\left(\delta_w - \tfrac{1}{2}\sin 2\delta_w\right). \tag{1}$$

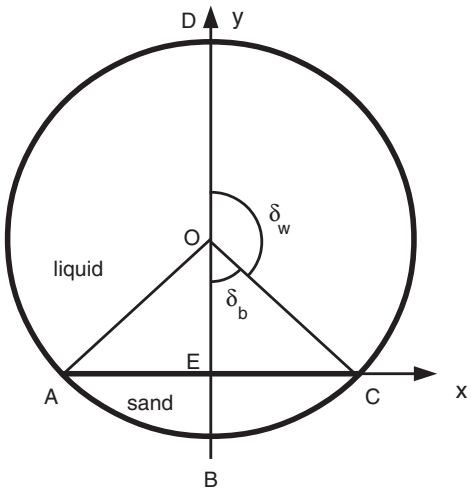

Fig. 1. Cross-section of the pipe, with sand at the bottom, and liquid above. The pipe has radius R and the maximum sand bed depth, EB, is h (3). The sand bed width AEC has length C_b, and the length of the wetted wall ADC is C_w (2).

In the cross-section, the length C_b of the sand bed, and the length C_w of the portion of the cylindrical wall wetted by liquid, are

$$C_b = 2R\sin\delta_b, \quad C_w = 2R\delta_w. \tag{2}$$

The maximum height of the sand bed, at $x = 0$, is

$$h = R(1 - \cos\delta_b) = R(1 + \cos\delta_w), \tag{3}$$

and we note for future use that

$$\frac{\partial A}{\partial h} = -C_b, \quad \frac{\partial C_b}{\partial h} = -2\cot\delta_w. \tag{4}$$

Particle velocities in the bedload layer are much smaller than the bulk fluid velocity, typically a fraction of the fluid velocity at a distance of one particle diameter above the bed at rest. Hence it is usual to calculate the fluid flow as if the wavy bottom were fixed (Charru et al., 2013), and the errors introduced by this approximation are small. The liquid therefore satisfies a no-slip boundary condition both at the bed/liquid interface and on the circular wall of the pipe.

Flow of two fluids in such a geometry has been well studied (Bentwich, 1964; Ranger and Davis, 1979; Brauner et al., 1996; Biberg and Halvorsen, 2000), because of its importance when pumping two fluids that have separated due to their density difference. If the viscosity of the lower fluid is taken to be infinite, this lower fluid becomes stationary, and the flow of the upper fluid corresponds to fluid flowing above a sand bed. We present a short summary of the analysis and analytic predictions for this case of a uniform flat bed in Appendix A. However, we shall eventually need to use numerical methods, and it is convenient to do so even for the simplest case of a uniform sand bed. The analytic results then provide a useful check on the accuracy of the numerical scheme.

The liquid is assumed to be Newtonian and incompressible, with density ρ and viscosity η. If the bed of sand is uniform, the liquid velocity w in the z direction satisfies

$$\left(\frac{\partial^2}{\partial x^2} + \frac{\partial^2}{\partial y^2}\right)w = -G/\eta, \tag{5}$$

where $-G < 0$ is the axial pressure gradient. We solved the Poisson Eq. (5), subject to a no slip condition at the boundaries, by means of the finite element package FreeFem++ (Hecht, 2012). By way of example, Fig. 2 shows isolines of the velocity $w(x, y)$, normalized by Q/R^2 where Q is the volumetric flow rate, for the case $h/R = 0.5$. Note that the maximum velocity is greater than the value $2/\pi$ for $h/R = 0$, as expected.

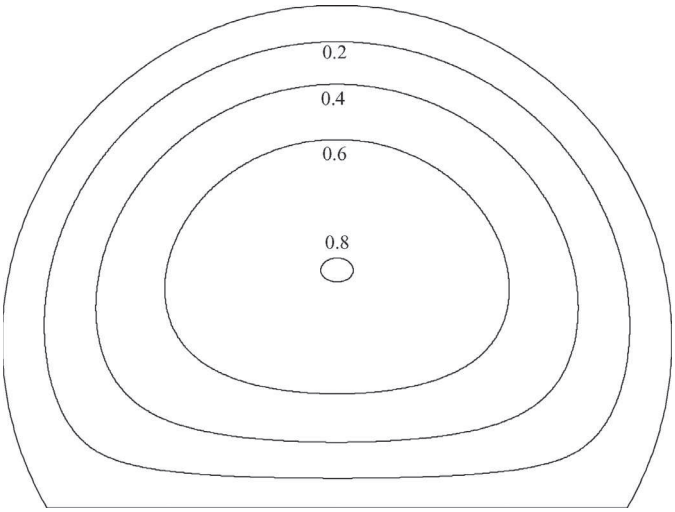

Fig. 2. Velocity field $w(x, y)$ normalized by Q/R^2 where Q is the flow rate, for $h/R = 0.5$. The FreeFem++ calculations used 24290 triangular elements.

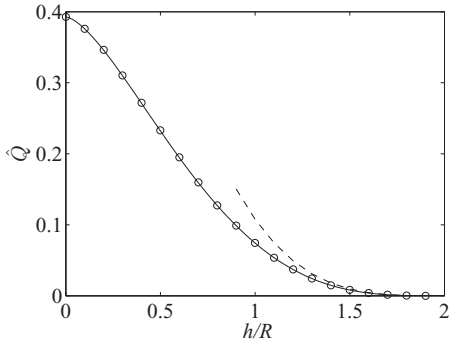

Fig. 3. Variation with h/R of the dimensionless flow rate $\hat{Q} = Q/(GR^4/\eta)$. (○), numerical solution; (—), analytical solution (7); (– –), asymptotic solution (115).

The computed dimensionless flow rate

$$\hat{Q} = \frac{Q}{GR^4/\eta}, \qquad Q = \int_A w \, \mathrm{d}S, \tag{6}$$

is shown in Fig. 3 as a function of h/R. This can be compared against the analytic result obtained by Ranger and Davis (1979), which takes the form

$$\hat{Q}(\delta_w) = \frac{\delta_w}{8} - \frac{\sin 2\delta_w}{24} - \frac{\sin 4\delta_w}{96} - \sin^4 \delta_w I \tag{7}$$

where

$$I = \int_0^\infty \frac{\pi \omega^3 \cosh \omega\delta_w \, \mathrm{d}\omega}{\sinh \omega\delta_w \sinh^2 \omega\pi}. \tag{8}$$

Details are given in Appendix A.2, and the finite element computations are accurate to within 0.02%. In the Appendix it is also shown that the integral I (8) is closely approximated by

$$I \approx I_{\text{small}} = \frac{1}{6\delta_w} + \frac{\delta_w}{90} - \frac{\delta_w^3}{1890} + \frac{\delta_w^5}{14175} + \cdots, \quad \delta_w \ll \pi. \tag{9}$$

When this approximation is inserted into the expression (7) for Q, the errors are less than 0.34% for all δ_w. The height h of the sand bed is related to the angle δ_w by the relation (3), and from now on we shall consider $\hat{Q}$ to be a function of h, rather than of δ_w. It is shown in Eq. (115) of A.2, that $\hat{Q} \sim (2 - h/R)^{7/2}$ as $h \to 2R$, as can be seen in Fig. 3.

The shear stress $\tau_b = \tau_{yz}$ over the sand bed C_b, and the shear stress $\tau_w = \tau_{rz}$ over the wetted wall C_w of the cylinder, are non-uniform. Computational results for these shear stresses, normalized by GR, are shown in Fig. 4. For $h/R = 0.25$ (small sand content), the bed shear stress τ_b varies strongly, with maximum value larger than $\frac{1}{2}GR$; τ_w is nearly uniform and close to the value $\frac{1}{2}GR$ (the classical value for Poiseuille flow), and decreases sharply as the sand bed is approached ($|\psi| \lesssim \delta_w$). For higher sand content ($h/R = 1$ and $h/R = 1.75$), both stresses are smaller than at low sand content, as expected (increasing bed height at constant pressure gradient corresponds to decreasing flow rate).

We shall later need the average shear stresses over the sand bed and wetted wall:

$$\overline{\tau}_b = \frac{1}{C_b} \int_{C_b} \tau_b \, \mathrm{d}x, \quad \overline{\tau}_w = \frac{R}{C_w} \int_{C_w} \tau_w \, \mathrm{d}\psi. \tag{10}$$

These mean shear stresses are discussed by Biberg and Halvorsen (2000) and details are given in Appendix A.3. In particular, on the sand bed,

$$\overline{\tau}_b = \frac{GR^2}{C_b} \left(\frac{\sin^2 \delta_w}{\delta_w} - \frac{\sin 2\delta_w}{2} \right) \tag{11}$$

and on the wetted wall

$$\overline{\tau}_w = \frac{GR^2}{C_w} \left(\delta_w - \frac{\sin^2 \delta_w}{\delta_w} \right). \tag{12}$$

Variations with h/R of $\overline{\tau}_b$ and $\overline{\tau}_w$ are shown in Fig. 5. For $h/R = 0$, the classical value $\frac{1}{2}GR$ is recovered. As the bed thickness increases, the stresses decrease (as does the flow rate), except for small h/R where $\overline{\tau}_b$ first slightly increases.

The mean liquid velocity $\overline{w}$ in the pipe is

$$\overline{w} = \frac{Q}{A} = \frac{1}{A} \int_A w \, \mathrm{d}S. \tag{13}$$

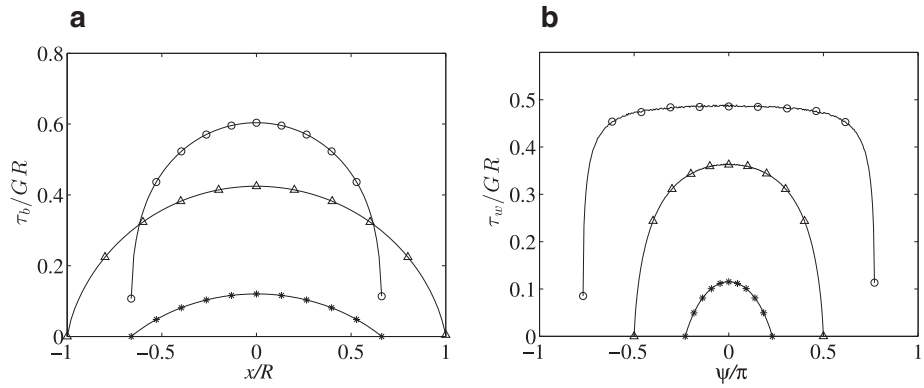

Fig. 4. Distribution of the shear stresses along the boundaries: (a), τ_b on the bed; (b), τ_w on the pipe wall. (○), $h/R = 0.25$; (△), $h/R = 1$; (∗), $h/R = 1.75$.

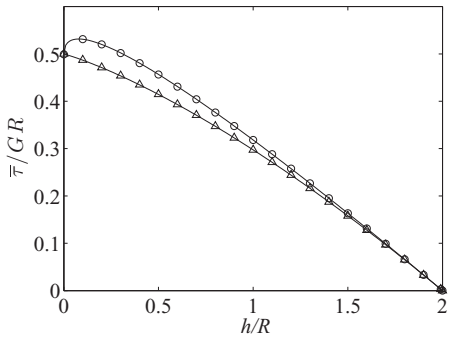

Fig. 5. Variation with h/R of the mean shear stresses (10) $\overline{\tau}_b$ (○) and $\overline{\tau}_w$ (△), normalised by GR. Symbols, numerical solution; (—), analytical solutions (11) and (12).

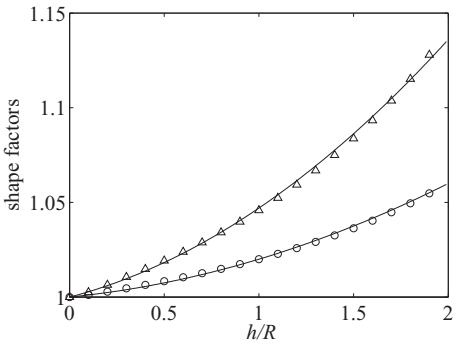

Fig. 6. Variations with h/R of the shape factors α (○) (14) and β (△) (16) of the velocity profile $w(x, y)$, normalized by $\alpha_{\rm ns} = 4/3$ and $\beta_{\rm ns} = 2$, their values for $h/R = 0$. Symbols, numerical solution; (—), fits (15) and (17).

The stability analysis of Section 6 requires the shape factor α of the profile of w^2 over the cross section, i.e.,

$$\alpha = \frac{1}{A\overline{w}^2}\int_A w^2\,\mathrm{d}S. \tag{14}$$

Results for α, scaled by the value $\alpha_{\rm ns} = 4/3$ for a pipe with no sand, are shown in Fig. 6 as a function of h/R. They vary little over the entire range of h, and may be approximated by

$$\frac{\alpha}{\alpha_{\rm ns}} = 1 + 0.01\left(\frac{h}{R}\right) + 0.01\left(\frac{h}{R}\right)^2. \tag{15}$$

The end point $\alpha(h = 2R) = 35/33$ can be found analytically (Appendix A.5). Similarly, we shall require the shape factor β of the profile of w^3:

$$\beta = \frac{1}{A\overline{w}^3}\int_A w^3\,\mathrm{d}S. \tag{16}$$

Results for β, scaled by the value $\beta_{\rm ns} = 2$ for a pipe with no sand, are shown in Fig. 6 and (like those for α) vary little over the entire range of h. They are approximated by

$$\frac{\beta}{\beta_{\rm ns}} = 1 + 0.021\left(\frac{h}{R}\right) + 0.026\left(\frac{h}{R}\right)^2. \tag{17}$$

The end point $\beta(h = 2R) = 490/429$ can again be found analytically (Appendix A.5).

3. A slowly varying sand bed

We now consider a sand bed with a height $h(z)$ that varies slowly as a function of the axial position z. A first approximation to the fluid velocity is given by the velocity w found in Section 2 at the appropriate local value of the height h of the sand bed. However, secondary flows must be established in order to allow the fluid velocity to evolve as it moves along the pipe. In particular, the streamlines will no longer be parallel to the pipe axis, and inertial effects are introduced: a standard example is Dean flow in a helical pipe (Berger et al., 1983).

We follow the exposition of Manton (1971) who considers flow through a circular pipe with diameter that varies slowly with position z along the pipe. The cross-sectional area of such a pipe changes, but not the shape. A related problem of flow through a pipe with an elliptical cross-section is studied by Todd (1977). The aspect ratio of the ellipse remains constant, but the ellipse axes rotate with position along the pipe. Thus the cross-sectional area of pipe remains constant, but the shape changes. In the partially sand-filled pipe considered here, both the shape and area of the cross-section change with position along the pipe.

In this Section, we choose the pipe radius R, the velocity $W = Q/R^2$ and the stress $\eta W/R$ as the length, velocity and pressure scales, respectively. Since the flow rate is constant along the pipe due to incompressibility, these scales are constant too, unlike the pressure gradient which varies slowly. The steady non-dimensional Navier–Stokes equations are

$$\mathrm{Re}(\mathbf{u}.\nabla)\mathbf{u} = -\nabla p + \nabla^2\mathbf{u}, \tag{18}$$

where

$$\mathrm{Re} = \frac{\rho RW}{\eta} = \frac{\rho Q}{R\eta} \tag{19}$$

is the Reynolds number.

We now assume that changes in the z direction (along the pipe axis) occur slowly over a lengthscale $O(R/\epsilon)$, where $\epsilon \ll 1$ is a typical bed slope. Since $W = Q/R^2$ is a typical fluid velocity in the axial (z) direction, velocities in the (x, y) directions are $O(\epsilon W)$ by continuity, and inertial corrections to the axial velocity field are $O(W\epsilon\mathrm{Re})$. Thus, we follow (Manton, 1971) and seek an expansion of the (dimensionless) fluid velocity and pressure in the form

$$\mathbf{u} = \mathbf{u}^{(0)} + h'\mathbf{u}^{(1s)} + h'\mathrm{Re}\,\mathbf{u}^{(1i)} + \cdots, \tag{20a}$$

$$p = p^{(0)} + h'p^{(1s)} + h'\mathrm{Re}\,p^{(1i)} + \cdots, \tag{20b}$$

where $h' = \mathrm{d}h/\mathrm{d}z$ is the local bed slope, $\mathbf{u}^{(0)}$ is the velocity in a uniform pipe, $h'\mathbf{u}^{(1s)} \sim O(\epsilon)$ is a Stokes flow correction due to incompressibility, and $h'\mathrm{Re}\,\mathbf{u}^{(1i)} \sim O(\epsilon\mathrm{Re})$ is the first inertial correction. Thus, as is usual in problems of nearly unidirectional flow, we require only that $\epsilon\mathrm{Re} \ll 1$ (subject, of course, to the Reynolds number being sufficiently small to avoid transition to turbulence).

The leading order solution consists of an axial flow $\mathbf{u}^{(0)} = (0, 0, w^{(0)})$, where w_0 satisfies the equation

$$\nabla_H^2 w^{(0)} = \frac{\partial p^{(0)}}{\partial z}, \tag{21}$$

where ∇_H^2 is the (dimensionless) two-dimensional Laplace operator

$$\nabla_H^2 = \frac{\partial^2}{\partial x^2} + \frac{\partial^2}{\partial y^2}. \tag{22}$$

We recover here the uniform flow problem discussed in Section 2, Eq. (5), whose dimensional solution is given in Appendix A1, Eq. (104), with pressure gradient $G(Q)$ given by (112), or, in dimensionless form:

$$\frac{\partial p^{(0)}}{\partial z} = -1/\hat{Q}. \tag{23}$$

In the present case of non-uniform flow, slow variations of the bed height along the pipe imply slow variations of $\hat{Q}(h/R)$ according to (7), and therefore slow variations of the pressure gradient (23).

To find the Stokes flow correction $\mathbf{u}^{(1s)} = (u^{(1s)}, v^{(1s)}, 0)$ associated with the slow changes in the z-direction of the velocity field

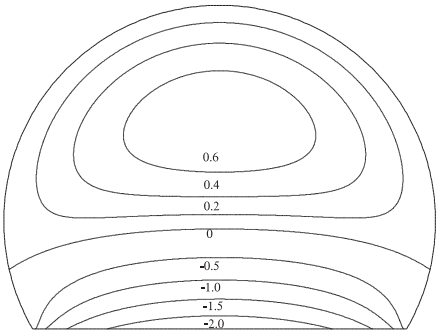

Fig. 7. Isolines of the velocity gradient $(h')^{-1}\partial w^{(0)}/\partial z$, normalized by Q/R^3, for $h/R = 0.5$.

$w^{(0)}$, we shall require the derivative $\partial w^{(0)}/\partial z$. One method to determine $\partial w^{(0)}/\partial z$ would be to differentiate the analytic expression (104), holding (x, y) constant. However, the results are unwieldy, and we again turn to numerical computation. Differentiating (21) with respect to z and using (23), we find

$$\nabla_H^2 \frac{\partial w^{(0)}}{\partial z} = \frac{\partial^2 p^{(0)}}{\partial z^2} = \frac{h'}{\hat{Q}^2}\frac{\mathrm{d}\hat{Q}}{\mathrm{d}h}, \tag{24}$$

where $\mathrm{d}\hat{Q}/\mathrm{d}h$ is obtained in terms of $\mathrm{d}I/\mathrm{d}\delta_w$ by differentiating (7). The derivative $\mathrm{d}I/\mathrm{d}\delta_w$ can be obtained from the exact integral form (8) for I. However, for computational purposes it is easier to differentiate the approximate expression (9) for I. The resulting approximation for $\mathrm{d}\hat{Q}/\mathrm{d}h$ has relative errors of at most 1.3%. The boundary conditions for (24) are

$$\frac{1}{h'}\frac{\partial w^{(0)}}{\partial z} = 0 \quad \text{on } C_w, \tag{25a}$$

$$= -\frac{\partial w^{(0)}}{\partial y} \quad \text{on } C_b. \tag{25b}$$

Thus $\partial w^{(0)}/\partial z$ satisfies a Poisson equation (24), and could be found by methods similar to those used in Appendix A to obtain w. However, we again choose to solve (24) by means of the finite element package FreeFem++. Fig. 7 shows $\left(h'\right)^{-1}\partial w^{(0)}/\partial z$. For positive bed slope, the flow is accelerated, except close to the bed where it slows down due to the approach of the no-slip bed boundary at which the fluid velocity is zero.

At $O(\epsilon)$, the Navier–Stokes equations become

$$\nabla_H^2 u^{(1s)} = \frac{\partial p^{(1s)}}{\partial x}, \quad \nabla_H^2 v^{(1s)} = \frac{\partial p^{(1s)}}{\partial y}, \tag{26}$$

with incompressibility in the (x, y) plane replaced by the forced equation

$$\frac{\partial u^{(1s)}}{\partial x} + \frac{\partial v^{(1s)}}{\partial y} = -\frac{1}{h'}\frac{\partial w^{(0)}}{\partial z}. \tag{27}$$

We require $u^{(1s)} = v^{(1s)} = 0$ on the boundary, which is consistent with (27) since incompressibility imposes that the integral

$$\int_A \frac{\partial w^{(0)}}{\partial z}\mathrm{d}S \tag{28}$$

over the cross-sectional area A of the liquid is zero. The above equations for the Stokes corrections $\mathbf{u}^{(1s)}$ and $p^{(1s)}$ were solved numerically by means of FreeFem++, and typical results for the velocities $u^{(1s)}$ and $v^{(1s)}$ are shown in Fig. 8. The vertical component $v^{(1s)}$ is positive and much larger than $u^{(1s)}$, so that, for $h' > 0$, the flow is predominantly upwards (no eddies). Close to the bed, the direction of the horizontal Stokes correction (and shear stress) depends on the bed height: for $h/R < 1$, the fluid pushed upwards by the rising bed ($h' > 0$) flows into the corners, so as to move sand grains from the center of the bed towards the walls (Fig. 8a), whereas for $h/R > 1$, the directions are reversed (Fig. 8c), with the transition between the two behaviors at $h/R = 1$.

Pressure gradients in the (x, y) plane are $O(\epsilon G)$. The non-uniform pressure $p^{(1s)}$ over the (x, y) plane varies slowly in the z direction, leading to axial pressure gradients that are non-uniform over the (x, y) plane only at $O(\epsilon^2\, G)$. They can therefore be neglected at the order to which we are working.

We now consider inertial effects. In particular, we shall require the inertial correction $w^{(1i)}$ to the axial velocity, which satisfies

$$\nabla_H^2 w^{(1i)} - \frac{\partial p^{(1i)}}{\partial z} = u^{(1s)}\frac{\partial w^{(0)}}{\partial x} + v^{(1s)}\frac{\partial w^{(0)}}{\partial y} + \frac{w^{(0)}}{h'}\frac{\partial w^{(0)}}{\partial z} \tag{29}$$

with boundary condition $w^{(1i)} = 0$ on both the pipe wall and the surface of the sand bed. Once again, incompressibility implies that the volumetric flow rate Q is fixed, and so the pressure gradient $\partial p^{(1i)}/\partial z$ in (29) must be chosen in such a way that the integral

$$\int_A w^{(1i)}\,\mathrm{d}S \tag{30}$$

is zero. An easy way to achieve this is first to solve (29) for $w_0^{(1i)}$ with $\partial p^{(1i)}/\partial z = 0$, and then to correct the volumetric flow rate by picking the pressure gradient to be

$$\frac{\partial p^{(1i)}}{\partial z} = \frac{G}{Q}\frac{R^4}{\eta}\int_A w_0^{(1i)}\,\mathrm{d}S = \frac{1}{\hat{Q}}\int_A w_0^{(1i)}\,\mathrm{d}S. \tag{31}$$

(As discussed above, the axial pressure gradient related to the Stokes secondary flow, $\partial p^{(1s)}/\partial z$, is of higher order.) The corresponding axial velocity is

$$w^{(1i)} = w_0^{(1i)} - w^{(0)}\int_A w_0^{(1i)}\,\mathrm{d}S. \tag{32}$$

Fig. 9 shows a typical velocity field for $w^{(1i)}$. The correction is negative in the core of the pipe, corresponding to the retarding effect of inertia in an accelerating flow, and positive near the boundaries in order to satisfy the zero net flux condition.

The dimensional shear stress on the sand bed and on the pipe wall can be written as

$$\frac{\eta W}{R}\left(\tau^{(0)} + h'\mathrm{Re}\,\tau^{(1i)}\right) = GR\hat{Q}\left(\tau^{(0)} + h'\mathrm{Re}\,\tau^{(1i)}\right) \tag{33}$$

where $\tau^{(0)}$ and $\tau^{(1i)}$ are non-dimensional stresses corresponding to the non-dimensional velocities $w^{(0)}$ and $w^{(1i)}$. However, stresses scaled by $\eta W/R = GR\hat{Q}$ become infinite as the bed fills with sand (i.e., as $h \to 2R$), in the same way as the non-dimensional unperturbed pressure gradient $1/\hat{Q}$ becomes infinite when $h \to 2R$ with the flow rate Q held constant. It is therefore more convenient to discuss the inertial stresses scaled by GR, rather than by $GR\hat{Q}$. This scaling, used previously in Figs. 4 and 5, allows us to directly compare the $O(\mathrm{Re})$ stress perturbations with the stresses in the unperturbed flow.

The bed shear stress $\tau_b^{(1i)}$ varies with position x across the bed, as does the wall shear stress $\tau_w^{(1i)}$ on the pipe wall. These variations are shown in Fig. 10 for various values of h/R, and are clearly related to the variations in axial velocity shown in Fig. 9.

The mean, scaled stress perturbation, averaged over the surface of the sand bed, is

$$\overline{\tau}_b^{(1)} = \frac{1}{C_b}\int_{C_b}\tau_b^{(1i)}\,\mathrm{d}x \tag{34}$$

and the mean, scaled stress over the wetted surface of the pipe is

$$\overline{\tau}_w^{(1)} = \frac{R}{C_w}\int_{C_w}\tau_w^{(1i)}\,\mathrm{d}\psi. \tag{35}$$

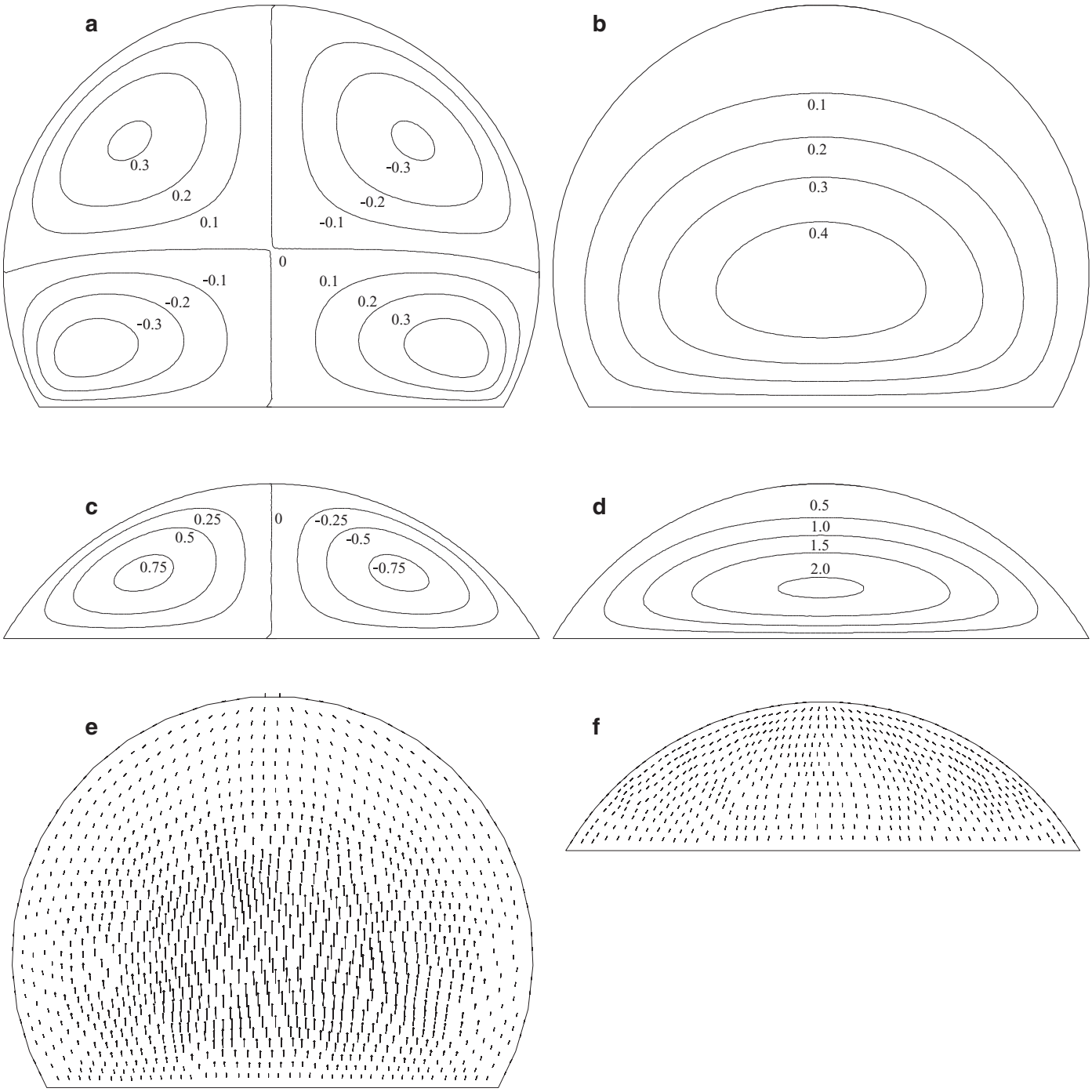

Fig. 8. Stokes correction to the parallel flow $w^{(0)}$. (a) and (b), isolines of $u^{(1s)}$ and $v^{(1s)}$, for $h/R = 0.5$; (c) and (d), $u^{(1s)}$ and $v^{(1s)}$ for $h/R = 1.5$; (e) and (f), velocity vectors corresponding to (a,b) and (c,d).

These mean stresses, together with the pressure gradient $\partial p^{(1i)}/\partial z$, are shown in Fig. 11. When the bed thickness h is small, the area of the bed increases as $h^{3/2}$: the mean inertial bed and wall stresses, and the inertial pressure gradient, are all small. When $h \to 2R$ and the bed is nearly full of sand, it is shown in Eq. (148) of Appendix A.5 that the stresses $\overline{\tau}_b^{(1)}$ and $\overline{\tau}_w^{(1)}$ are equal and decrease as $(2 - h/R)^{1/2}$, whereas the perturbation pressure gradient $\partial p^{(1i)}/\partial z$ diverges as $(2 - h/R)^{-1/2}$, as shown in Eq. (146). We see from Fig. 11 that there is good agreement between the FreeFem++ numerical computations of the perturbed stresses and the asymptotic expressions when $2 - h/R \ll 1$. When FreeFem++ was used in Section 2 to determine the fluid velocity $w^{(0)}$ above a uniform sand bed, we could assess the accuracy of the results by comparing them against the analysis of Appendices A.1–A.3. In general we have no analytic results by which we might assess the accuracy of the computed inertial corrections (other than in the limit $2 - h/R \ll 1$). However, taking $h/R = 0.5$ as an example, we note that a reduction of the number of triangular elements used by FreeFem++ from 24290 to 6182 changed the computed inertial pressure gradient and mean wall and bed stresses by less than 0.06%.

Finally, we consider the ratio of the inertial force on the sand bed to the total inertial force on the bed and wetted cylinder wall,

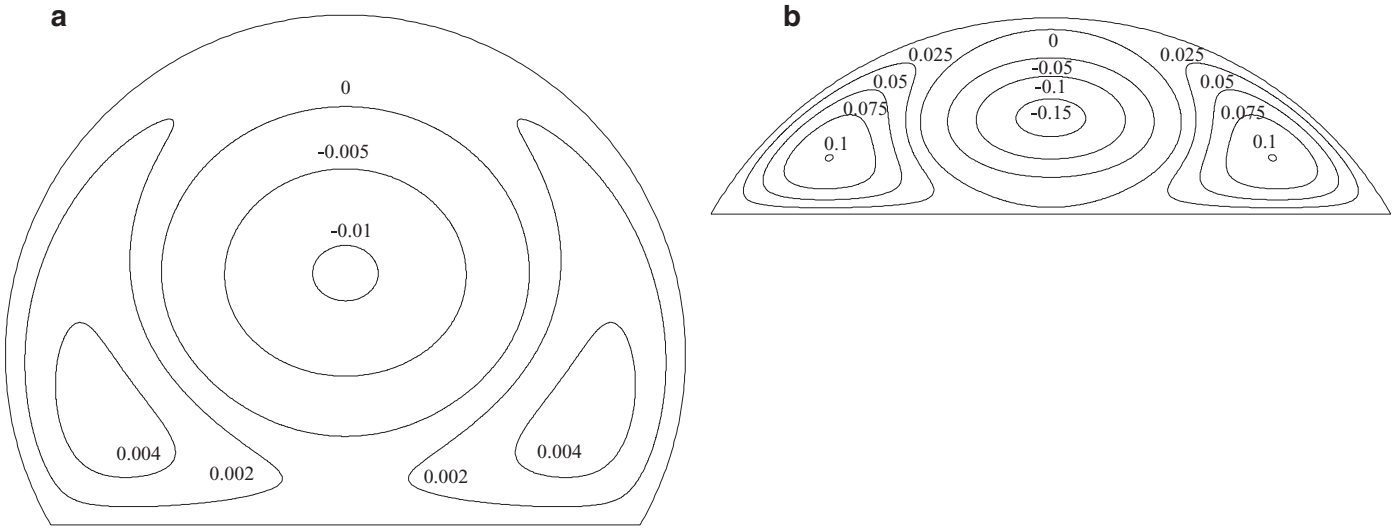

Fig. 9. Isolines of the inertial correction $w^{(1i)}$: (a), $h/R = 0.5$; (b), $h/R = 1.5$.

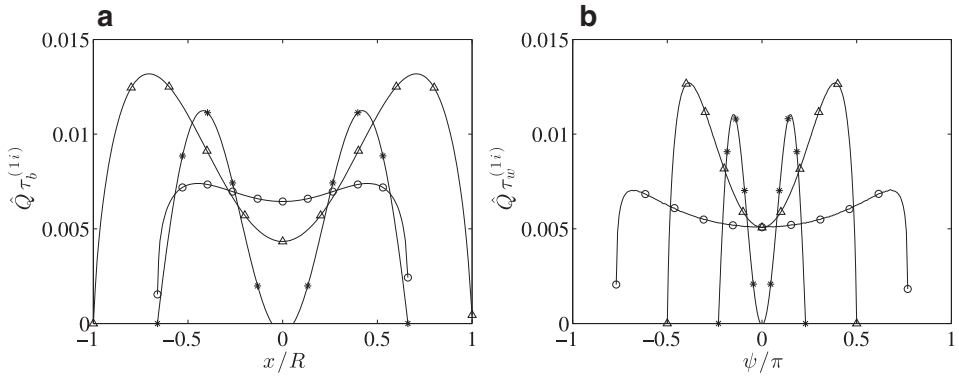

Fig. 10. Variation in the cross-section of the pipe of the inertial shear stresses, scaled by $h'\mathrm{Re}\,GR$. (a), across the bed; (b), on the pipe wall. (○), $h/R = 0.25$; (△), $h/R = 1$; (∗), $h/R = 1.75$.

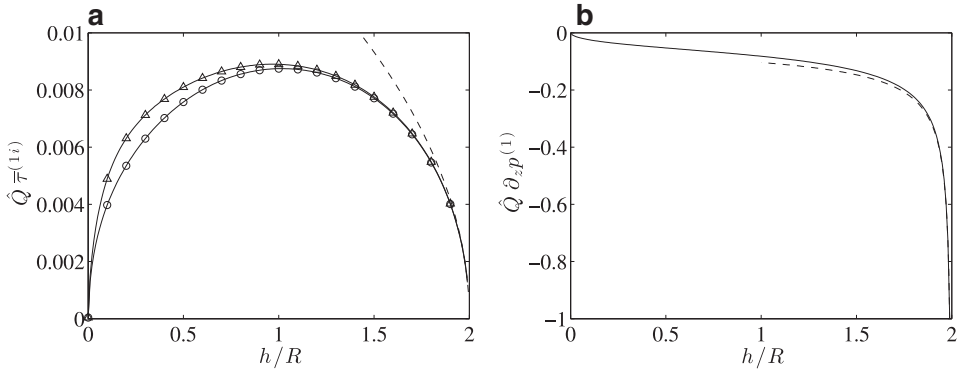

Fig. 11. Variations with h/R of the inertial corrections. (a) Mean shear stresses scaled by $h'\mathrm{Re}\,GR$: △, computed bed stress $\overline{\tau}_b^{(1)}$ (34); ○, computed wall stress $\overline{\tau}_w^{(1)}$ (35); (−−), asymptotic prediction (148) for $\delta_w \ll 1$. (b) Pressure gradient $\partial p^{(1)}/\partial z$ scaled by $h'\mathrm{Re}\,G$: (−), computed (31); (−−), asymptotic prediction (146) for $\delta_w \ll 1$.

$$\frac{C_b\overline{\tau}_b^{(1)}}{C_b\overline{\tau}_b^{(1)} + C_w\overline{\tau}_w^{(1)}}, \tag{36}$$

and compare this to the ratio of the Stokes forces, i.e., by (11) and (12),

$$\frac{C_b\overline{\tau}_b^{(0)}}{C_b\overline{\tau}_b^{(0)} + C_w\overline{\tau}_w^{(0)}} = \frac{2\sin^2\delta_w - \delta_w\sin 2\delta_w}{2\delta_w^2 - \delta_w\sin 2\delta_w}. \tag{37}$$

Fig. 12(a) shows that the ratios (36) and (37) remain close indeed, over the whole range of h/R. It can be seen that as h/R tends to 2, both force ratios tend to 0.5: in this limit the geometry is approaching that of a long narrow slot, for which we know that the stresses on the top and bottom are equal (Luchini and Charru, 2010a), hence the ratio 0.5. This result is also consistent with the analytic results (130) for the unperturbed flow (A.3), and (148) for the inertial perturbation (A.5). A more quantitative demonstration of the closeness of the force ratios is obtained from Fig. 12(b)

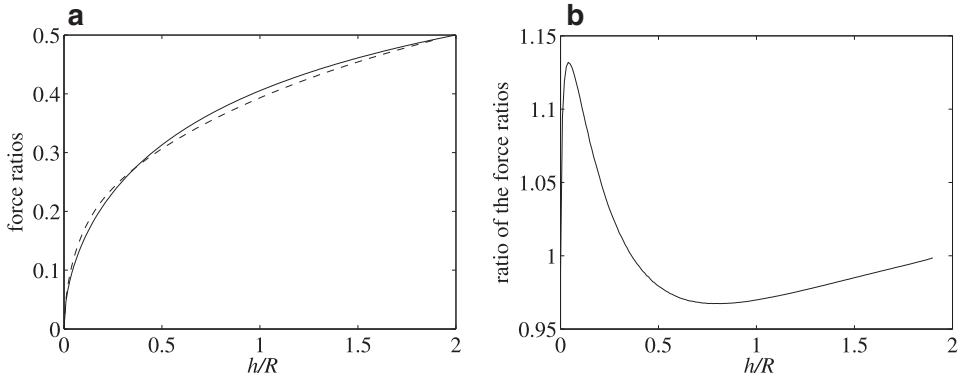

Fig. 12. (a) Variation with h/R of the inertial perturbed force ratio (36) (−−), and unperturbed force ratio (37) (−). (b) Variation with h/R of the ratio of the force ratios (38).

which displays the ratio of (36) to (37),

$$\frac{C_b\overline{\tau}_b^{(1)}}{C_b\overline{\tau}_b^{(1)}+C_w\overline{\tau}_w^{(1)}}\frac{C_b\overline{\tau}_b^{(0)}+C_w\overline{\tau}_w^{(0)}}{C_b\overline{\tau}_b^{(0)}}, \tag{38}$$

as a function of h/R. We see that it is close to one over the whole range of h/R. Thus, strikingly, the ratio of the mean inertial stress on the bed to that on the wall can be accurately estimated from the leading-order calculations.

4. Sand transport

We first review the theory of sand transport under a plane flow, i.e. for fluid flow in the z-direction above a plane sand bed $y = 0$, with no variation in the spanwise x-direction, as discussed by Charru et al. (2013). We assume that the sand particles are spherical, with diameter d, density ρ_p, and Stokes sedimentation velocity

$$V_\mathrm{fall} = \frac{(\rho_\mathrm{p}-\rho)gd^2}{18\eta}, \tag{39}$$

where g is the acceleration due to gravity.

It is known from experiment that sand particles on the bed surface do not move unless the shear stress τ_b acting on the bed exceeds a critical value, i.e., unless

$$\theta = \frac{\tau_b}{(\rho_\mathrm{p}-\rho)gd} > \theta_t, \tag{40}$$

where the dimensionless bed shear stress θ is known as the Shields number. For a horizontal bed, the critical Shields number $\theta_t = \theta_{t0} \approx 0.12$ (Charru et al., 2004; Ouriemi et al., 2009a). For a non-zero bed slope $\partial h/\partial z$, gravity pulls the grains downhill, and this effect may be included by modifying the critical Shields number to

$$\theta_t = \theta_{t0}\left(1+\cot(\chi)\frac{\partial h}{\partial z}\right), \tag{41}$$

where $\chi \approx 25°$ is the effective friction angle of the grains (Fredsøe, 1974).

If $\theta > \theta_t$ the grains move, and there is a flux q of grains in the flowing bedload (per unit length in the x direction). When equilibrium is achieved, the volume flux q of the particles (per unit bed width) saturates to Charru et al. (2004)

$$q_\mathrm{sat} = \frac{c_q}{1-\phi}\left(\frac{\pi d^3}{6}\right)\frac{V_\mathrm{fall}}{d^2}\,\theta(\theta-\theta_t), \quad \theta_t < \theta, \tag{42a}$$

$$= 0, \quad 0 < \theta < \theta_t, \tag{42b}$$

with $c_q = 0.85$ in the experiments and where the inclusion of the bed solid volume fraction $(1-\phi)$ slightly simplifies the subsequent equations.

If the wall shear stress τ_b varies in time or space, the particle flux q differs from the local equilibrium value, though usually not by much. The relaxation of the particle flux towards the new equilibrium can therefore be described by a linear equation

$$T_\mathrm{sat}\frac{\partial q}{\partial t} + L_\mathrm{sat}\frac{\partial q}{\partial z} = q_\mathrm{sat}(\tau_b) - q, \tag{43}$$

where t is time, T_sat is the saturation time and L_sat the saturation length. The saturation time scale T_sat is rapid (typically 1 s) compared to the timescale for the growth of instabilities of the bed: we therefore set this term to zero, so that

$$L_\mathrm{sat}\frac{\partial q}{\partial z} = q_\mathrm{sat}(\tau_b) - q. \tag{44}$$

The concept of a saturation length L_sat dates back to Bagnold (1941, 1979) (see e.g., Andreotti et al., 2013). The saturation length L_sat is poorly characterized. Following Charru (2006) we assume that it is given by the deposition length

$$L_\mathrm{sat} = c_L\frac{\gamma d}{V_\mathrm{fall}}\,d, \tag{45}$$

with $c_L = 1.5$ from the experiments of Charru et al. (2004) and where γ is the shear rate at the bed. Finally, mass conservation of the layer of moving grains (known as the Exner equation) gives (for plane flow),

$$\frac{\partial h}{\partial t} + \frac{\partial q}{\partial z} = 0. \tag{46}$$

For the present case of pipe flow, both the shear stress on the bed and the particle flux vary in the spanwise x-direction. Nevertheless, to be consistent with the simplification that the interface between the sand bed and the liquid is plane, we assume that the dependence of the mean particle flux in the z-direction, $\overline{q}_\mathrm{sat}$, on the mean shear stress $\overline{\tau}_b$ is still given by (42), *i.e.*, $\overline{q}_\mathrm{sat} = q_\mathrm{sat}(\overline{\tau}_b)$. Then, for pipe flow, the mass conservation Eq. (46) becomes

$$-\frac{\partial A}{\partial t} + \frac{\partial(C_b\overline{q})}{\partial z} = 0, \tag{47}$$

or, using Eqs. (2)–(4),

$$\frac{\partial h}{\partial t} + \frac{\partial \overline{q}}{\partial z} - \frac{h'}{R}\frac{\cot\delta_w}{\sin\delta_w}\,\overline{q} = 0, \tag{48}$$

where $h' = \partial h/\partial z$ is the bed slope. The last term in (48) accounts for the variation of C_b with h (or δ_w). Note that this term is zero for a half-filled pipe ($\delta_w = \pi/2$).

5. Area-averaged equations

As in Section 3, we nondimensionalize lengths by R, velocities by $W = Q/R^2$, stresses by $\eta W/R = \eta Q/R^3$, and time by R^3/Q, and use the Reynolds number $\mathrm{Re} = \rho W R/\eta$ (19). We still assume that the surface of the perturbed bed remains horizontal in the cross-sectional (x, y) plane, so that the bed height h is a function only of the z-coordinate along the axis of the pipe.

5.1. Consistent area-averaged equations

Averaging the conservation equations over the section of the pipe provides a useful set of simplified equations governing the slow variations of two-phase flows, see *e.g.*, Lin and Hanratty (1986). Such equations are widely used in engineering applications. However, the averaging process loses information, so that some closure law for the shear stress must be introduced. The closure law may be empirical, or taken from the calculation of the first-order correction of the leading-order parallel flow, using an expansion of the dependent variables in terms of the small-slope parameter $\epsilon = h'$. We follow here an alternative method proposed by Luchini and Charru (2010a, 2010b), which provides consistent equations (correct to first-order) without the need for full first-order calculations. However, a difficulty arises in the pipe flow considered here because the method of Luchini and Charru gives the total integral of the boundary shear stress acting on the fluid but is unable to distinguish the separate contributions of the wall and bed stresses. The separation of these two contributions will be handled by an approximation discussed in Section 5.2.

The equations of continuity, axial momentum, and kinetic energy, when averaged over the cross-sectional area A of the liquid, are

$$\frac{\partial A}{\partial t} + \frac{\partial}{\partial z}\int_A w\,\mathrm{d}S = 0, \tag{49}$$

$$\mathrm{Re}\frac{\partial}{\partial t}\int_A w\,\mathrm{d}S + \mathrm{Re}\frac{\partial}{\partial z}\int_A w^2\,\mathrm{d}S = -\int_A \frac{\partial p}{\partial z}\,\mathrm{d}S - C_w\overline{\tau}_w - C_b\overline{\tau}_b, \tag{50}$$

and

$$\frac{\mathrm{Re}}{2}\frac{\partial}{\partial t}\int_A w^2\,\mathrm{d}S + \frac{\mathrm{Re}}{2}\frac{\partial}{\partial z}\int_A w^3\,\mathrm{d}S = -\int_A w\frac{\partial p}{\partial z}\,\mathrm{d}S - F, \tag{51}$$

where

$$F = -\int_A \mathbf{u}.\nabla^2\mathbf{u}\,\mathrm{d}S = \int_A (\nabla\mathbf{u}) : (\nabla\mathbf{u})\,\mathrm{d}S \tag{52}$$

is the rate of dissipation of energy per unit length of the pipe.

At leading order in the small-slope parameter ϵ, Eqs. (49)–(51) are satisfied by uniaxial flow with velocity $w^{(0)}$ over a sand bed of uniform depth h equal to the local bed depth, as discussed in Section 2. We now seek corrections to this flow caused by slow $O(\epsilon)$ changes in the bed depth. When working to $O(\epsilon)$, it suffices to approximate the integrals on the left-hand sides of Eqs. (49)–(51) by an integral of the steady axial velocity $w^{(0)}$ at the local bed depth h and local volumetric flow rate,

$$\overline{w} = \frac{1}{A}\int_A w^{(0)}\,\mathrm{d}S \tag{53}$$

together with shape coefficients α (14) and β (16) of the unperturbed velocity profile:

$$\alpha = \frac{1}{A\overline{w}^2}\int_A \left(w^{(0)}\right)^2\mathrm{d}S, \quad \beta = \frac{1}{A\overline{w}^3}\int_A \left(w^{(0)}\right)^3\mathrm{d}S. \tag{54}$$

Note that changes in the bed height $h(z, t)$ with time lead to changes in the local volumetric volume flow rate, so that $\overline{w}A$ is not necessarily equal to 1.

We saw in Section 3 that $\partial p/\partial z$ is a function only of z at $O(\epsilon)$ and is independent of (x, y), and can therefore be taken outside the integrals on the right-hand sides of Eqs. (50)–(51). The averaged Eqs. (49)–(51) therefore simplify to

$$\frac{\partial A}{\partial t} + \frac{\partial(A\overline{w})}{\partial z} = 0, \tag{55}$$

$$\mathrm{Re}\frac{\partial(A\overline{w})}{\partial t} + \mathrm{Re}\frac{\partial(\alpha A\overline{w}^2)}{\partial z} = -A\frac{\partial p}{\partial z} - C_w\overline{\tau}_w - C_b\overline{\tau}_b, \tag{56}$$

and

$$\frac{\mathrm{Re}}{2}\frac{\partial(\alpha A\overline{w}^2)}{\partial t} + \frac{\mathrm{Re}}{2}\frac{\partial(\beta A\overline{w}^3)}{\partial z} = -A\overline{w}\frac{\partial p}{\partial z} - F, \tag{57}$$

correct to $O(\epsilon)$.

Any attempt to work solely with the averaged equations of continuity (55) and momentum (56) to determine variations in the pressure gradient requires some semi-empirical closure law for the shear stresses in (56), and such closure laws do not usually correctly capture the $O(\epsilon)$ change in the stress. For example, the resulting dispersion relation for free surface waves of infinitesimal amplitude is wrong (Luchini and Charru, 2010a). The shear stresses on our bed of sand in a pipe may be obtained, of course, from the $O(\epsilon)$ calculations of Section 2. However, Luchini and Charru (2010a) showed that if we appeal to the averaged energy Eq. (57) in addition to the averaged equations of continuity (55) and momentum (56), the equations yield the pressure gradient and total shear force at the wall, correct to $O(\epsilon)$. The analysis relies on the fact that the rate of energy dissipation in a bounded domain with specified boundary conditions is minimized by the Stokes flow satisfying the boundary conditions, so that the $O(\epsilon)$ perturbation to the dissipation F on the right hand side of (57) is zero. To see this explicitly, we first note that $\nabla^2 = \partial_z^2 + \nabla_H^2$, where ∇_H^2 is the Laplace operator in the cross-sectional (x, y) plane and $\partial_z^2\mathbf{u}$ is $O(\epsilon^2)$. Contributions to F from the velocity components in the cross-sectional plane are similarly $O(\epsilon^2)$. We consider an axial velocity field $w = w^{(0)} + \delta w$, where δw satisfies the no-slip boundary condition on the pipe walls and sand bed surface, and has cross-sectional average $\int_A \delta w\,\mathrm{d}S = 0$, by (53). The dissipation F (52) can therefore be expressed as

$$\begin{aligned} F &= \int_A \left[\nabla_H w^{(0)}.\nabla_H w^{(0)} + 2\nabla_H\delta w.\nabla_H w^{(0)}\right]\mathrm{d}S + O(\epsilon^2) \\ &= -\int_A \left[w^{(0)}\nabla_H^2 w^{(0)} + 2\delta w\nabla_H^2 w^{(0)}\right]\mathrm{d}S + O(\epsilon^2) \\ &= -\overline{w}\frac{\partial p^{(0)}}{\partial z} + O(\epsilon^2), \end{aligned} \tag{58}$$

since $\nabla_H^2 w^{(0)} = \partial p^{(0)}/\partial z$ is uniform over the cross-section of the pipe. Thus, up to first-order, the dissipation rate depends only on the leading-order parallel-flow solution, so that the pressure gradient up to first-order is provided by the kinetic-energy Eq. (57) and the leading-order parallel flow.

We now have three equations (55)–(57), valid to $O(\epsilon)$, for $\overline{w}$, $\partial p/\partial z$ and for the total shear force $C_w\overline{\tau}_w + C_b\overline{\tau}_b$ on the boundary of the fluid. However, the motion of particles on the surface of the bed of sand depends upon τ_b, and not on the total shear force $C_w\overline{\tau}_w + C_b\overline{\tau}_b$. An approximation that allows us to obtain $\overline{\tau}_b$ from $C_w\overline{\tau}_w + C_b\overline{\tau}_b$ will be discussed in the next section.

5.2. Simplifying approximations

5.2.1. Quasi-static flow

A general feature of the dynamics of sand beds is that the time scale for evolution of the bed is much larger than that for changes in the flowing fluid. The fluid flow can therefore be regarded as quasistatic, and all time derivatives in the fluid equations neglected. The averaged equation of continuity (55) simplifies to become

$$A\overline{w} = 1 \tag{59}$$

so that the volumetric flow rate is uniform along the pipe (and equal to unity with our choice of the velocity and length scales).

The shape factors α and β and are well-fitted by the correlations (15) and (17) shown in Fig. 6 and vary only slowly with h. Since h varies only slowly with z, the variation of α and β with z is very slow indeed, and can be neglected. As a result, these shape factors can be moved outside the derivatives in (56) and (57), and when the time derivatives are neglected due to quasi-static flow, these equations become

$$\mathrm{Re}\,\alpha\frac{\partial\overline{w}}{\partial z}=-A\frac{\partial p}{\partial z}-C_w\overline{\tau}_w-C_b\overline{\tau}_b, \tag{60}$$

$$\frac{\partial p}{\partial z}=\frac{\partial p^{(0)}}{\partial z}-\beta\frac{\mathrm{Re}}{2}\frac{\partial\overline{w}^2}{\partial z}. \tag{61}$$

To obtain Eq. (60) a term $\overline{w}\frac{\partial\alpha}{\partial z}$ has been assumed negligibly small compared to $\alpha\frac{\partial\overline{w}}{\partial z}$, which requires

$$\left|\frac{1}{A}\frac{\mathrm{d}\alpha}{\mathrm{d}h}\right|\ll\left|\frac{1}{\alpha}\frac{\mathrm{d}A}{\mathrm{d}h}\right|=\left|\frac{C_b}{A}\right|. \tag{62}$$

Since the left-hand side of (62) is typically 0.01, (see the curve fit (15)), we see that (62) holds except when $\delta_w\sim 0.01$ and the pipe is almost full of sand. The neglect of the variation of β with z in (61) can be justified similarly. Note that the energy Eq. (61) implies that the viscous pressure gradient $\partial p^{(0)}/\partial z$ is merely modified by a Bernoulli term, which, using (59), can be written as

$$\beta\frac{\mathrm{Re}}{2}\frac{\partial\overline{w}^2}{\partial z}=\beta\frac{\mathrm{Re}}{A^3}\frac{\partial\overline{A}}{\partial z}=h'\mathrm{Re}\frac{\partial p_{\mathrm{av}}^{(1)}}{\partial z}, \tag{63}$$

where $h'=dh/dz$ is the local bed slope and where we have used (4) to define

$$\frac{\partial p_{\mathrm{av}}^{(1)}}{\partial z}=-\frac{\beta}{A^3}\frac{\partial A}{\partial h}=\frac{\beta C_b}{A^3}. \tag{64}$$

The above approximations may be assessed by comparing the above scaled pressure gradient with the exact first-order perturbation $\partial p^{(1)}/\partial z$ computed numerically in Section 3. The comparison is shown in Fig. 13. Pressure gradients at constant Q become infinite as $h\to 2$, and Fig. 13 has therefore been plotted to show $\hat{Q}\partial p_{\mathrm{av}}^{(1)}/\partial z$ and $\hat{Q}\partial p^{(1)}/\partial z$. This is equivalent to considering flow at fixed pressure gradient rather than at fixed volumetric flux.

We see in Fig. 13 that the pressure gradients determined via the two routes are all but indistinguishable, the minor differences originating in the neglect of the small term $\partial\beta/\partial z$ and use of the approximate correlations (15) and (17).

5.2.2. The ratio of the force $C_b\overline{\tau}_b$ on the bed to the force $C_w\overline{\tau}_w$ on the wetted wall

Eliminating the pressure gradient in the momentum Eq. (60) by means of (61), we find the total shear force on the cylinder wall and sand bed

$$C_w\overline{\tau}_w+C_b\overline{\tau}_b=-A\frac{\partial p^{(0)}}{\partial z}+\mathrm{Re}(\beta-\alpha)\frac{\partial\overline{w}}{\partial z}. \tag{65}$$

The first term on the right-hand side of (65) is the leading-order force. The second term is the inertial correction, and we emphasize that this term involves only leading-order quantities. However, the area-averaged equation (65) tells us only about the inertial correction to the *sum* of the forces on the sand bed and on the wetted cylinder wall. In a plane channel, it is known (by symmetry) that the change in stress is shared equally over the top and bottom of the channel, but here we have no such simplification. We propose to estimate the inertial correction of $\overline{\tau}_b$ by assuming that the ratio of the forces on the bed and the wetted wall, $C_b\overline{\tau}_b/C_w\overline{\tau}_w$, is the same as the ratio of the leading order forces, $C_b\overline{\tau}_b^{(0)}/C_w\overline{\tau}_w^{(0)}$, as

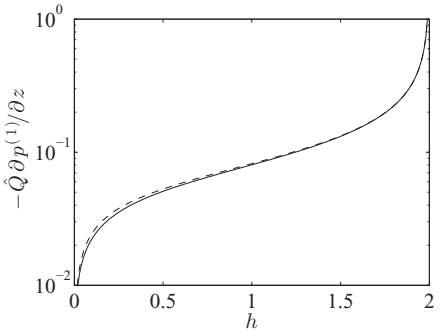

Fig. 13. Scaled pressure gradient perturbation against bed depth h. —-, $-\hat{Q}\partial p_{\mathrm{av}}^{(1)}/\partial z$ (64); - - -, $-\hat{Q}\partial p^{(1)}/\partial z$ computed numerically.

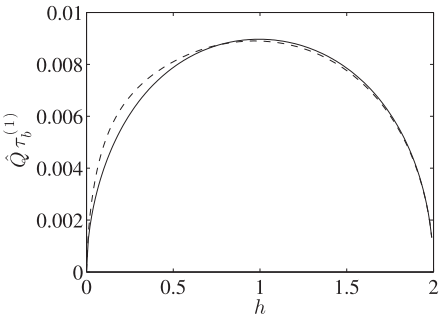

Fig. 14. Scaled inertial bed stress perturbation against bed depth h. —- $\overline{\tau}_{b,\mathrm{av}}^{(1)}$ (67); - - -, $\overline{\tau}_b^{(1)}$ computed numerically.

given by (37). With this assumption, the inertial correction to the bed shear stress is

$$h'\mathrm{Re}\,\overline{\tau}_{b,\mathrm{av}}^{(1)}=\frac{\overline{\tau}_b^{(0)}\,\mathrm{Re}\,(\beta-\alpha)}{C_b\overline{\tau}_b^{(0)}+C_w\overline{\tau}_w^{(0)}}\frac{\partial\overline{w}}{\partial z}, \tag{66}$$

from which, using (59) and (4), we find

$$\overline{\tau}_{b,\mathrm{av}}^{(1)}=\frac{\beta-\alpha}{A^2}\frac{C_b\overline{\tau}_b^{(0)}}{C_b\overline{\tau}_b^{(0)}+C_w\overline{\tau}_w^{(0)}}=(\beta-\alpha)\frac{4(2\sin^2\delta_w-\delta_w\sin 2\delta_w)}{\delta_w(2\delta_w-\sin 2\delta_w)^3}. \tag{67}$$

Fig. 14 compares the above shear stress $\overline{\tau}_{b,\mathrm{av}}^{(1)}$ with the exact first-order correction $\overline{\tau}_b^{(1)}$ as computed numerically in Section 3, with both curves multiplied by $\hat{Q}$ as in Fig. 13. The agreement is excellent, except for $h<0.5$. This is the range of h for which the approximation that the ratio of the perturbed bed and wall stresses equals the ratio of the zeroth-order bed and wall stresses is poorest (see Fig. 12).

6. Sand bed dynamics and stability

6.1. The equations governing sand bed dynamics

We collect together here the set of area-integrated equations governing the sand bed dynamics, for slow variations of the bed surface. We emphasize that these equations are consistent up to $O(\epsilon)$ and that they involve only the leading-order, parallel flow solution of the full problem. The equations have been non-dimensionalized using the length, velocity and stress scales introduced at the beginning of Section 5, together with the Reynolds number (19). Within the quasistatic assumption, incompressibility (59) implies

$$A\overline{w}=1, \tag{68}$$

and gives the mean velocity $\overline{w}(z)$ for given bed profile $h(z)$, via the geometric relations (1–3). The kinetic-energy equation then provides the pressure gradient (61)

$$\frac{\partial p}{\partial z} = \frac{\partial p^{(0)}}{\partial z} - \beta \frac{\mathrm{Re}}{2} \frac{\partial \overline{w}^2}{\partial z}, \tag{69}$$

where the leading-order pressure gradient $\partial p^{(0)}/\partial z = -1/\hat{Q}(\delta_w)$ is obtained from Eqs. (7)–(9). The momentum equation then provides the total force on the pipe wall and sand bed (65)

$$C_w \overline{\tau}_w + C_b \overline{\tau}_b = -A \frac{\partial p^{(0)}}{\partial z} + \mathrm{Re}(\beta - \alpha) \frac{\partial \overline{w}}{\partial z}, \tag{70}$$

with the shape coefficients α and β taken from the correlations (15) and (17).

In order to predict motion of the sand bed, we need to know the stress $\overline{\tau}_b = \overline{\tau}_b^{(0)} + h' \mathrm{Re} \overline{\tau}_{b,\mathrm{av}}^{(1)}$ acting on the bed, rather than the total viscous force $C_w \overline{\tau}_w + C_b \overline{\tau}_b$ acting on the bed and wetted pipe wall. But the stress $\overline{\tau}_b^{(0)}$ over a flat bed is known from (11):

$$\overline{\tau}_b^{(0)} = \frac{1}{2\hat{Q}(\delta_w)} \left(\frac{\sin \delta_w}{\delta_w} - \cos \delta_w \right), \tag{71}$$

and the approximation discussed in Section 5.2 gives us the stress perturbation (67) due to the non-zero slope:

$$\overline{\tau}_{b,\mathrm{av}}^{(1)} = (\beta - \alpha) \frac{4(2\sin^2 \delta_w - \delta_w \sin 2\delta_w)}{\delta_w (2\delta_w - \sin 2\delta_w)^3}. \tag{72}$$

We now turn to the equations governing the slow time evolution of the sand bed, as presented in Section 4. Mass conservation of the bedload layer (48) gives

$$\frac{\partial h}{\partial t} + \frac{\partial \overline{q}}{\partial z} - h' \frac{\cot \delta_w}{\sin \delta_w} \overline{q} = 0, \tag{73}$$

where $\overline{q}$ is the sand flux per unit bed width (non-dimensionalised by Q/R). This flux obeys the relaxation Eq. (44)

$$L_{\mathrm{sat}} \frac{\partial \overline{q}}{\partial z} = q_{\mathrm{sat}}(\overline{\tau}_b) - \overline{q}, \tag{74}$$

with the dimensionless saturation length (45)

$$L_{\mathrm{sat}} = c_L \overline{\tau}_b \frac{(d/R)^2}{V_{\mathrm{fall}}/W}, \tag{75}$$

and the empirical saturated sand flux (42)

$$\frac{q_{\mathrm{sat}}}{q_{\mathrm{ref}}} = \frac{\overline{\tau}_b}{\tau_{\mathrm{ref}}} \left(\frac{\overline{\tau}_b}{\tau_{\mathrm{ref}}} - \theta_{t0}(1 + h' \cot \chi) \right), \tag{76}$$

where

$$q_{\mathrm{ref}} = \frac{c_q \pi}{6(1-\phi)} \frac{V_{\mathrm{fall}} d}{WR}, \quad \tau_{\mathrm{ref}} = \frac{(\rho_{\mathrm{p}} - \rho) g d}{\eta W/R},$$
$$\theta_{t0} = 0.12, \quad \chi = 25^\circ. \tag{77}$$

An illustration of the use of the above equations is given in the next section.

6.2. Stability of the flat sand bed

The above fluid and particle equations admit a steady and uniform solution, with height h_0, bed shear stress $\tau_0 = \overline{\tau}_b^{(0)}(h_0)$, and particle flux $q_0 = q_{\mathrm{sat}}(\tau_0)$. We now consider that this base solution is perturbed so that the bed height is given by the real part of

$$h = h_0 + \epsilon h_1 \mathrm{e}^{\mathrm{i}k(z-ct)}. \tag{78}$$

The mean stress on the bed becomes

$$\overline{\tau}_b = \overline{\tau}_b^{(0)}(h) + h' \mathrm{Re}\, \overline{\tau}_{b,\mathrm{av}}^{(1)}(h) \tag{79}$$

$$= \tau_0 + \epsilon \tau_1 \mathrm{e}^{\mathrm{i}k(z-ct)} + \text{higher order terms}, \tag{80}$$

with

$$\tau_1 = \left(\left. \frac{\partial \overline{\tau}_b^{(0)}}{\partial h} \right|_Q + \mathrm{i}k\mathrm{Re}\, \overline{\tau}_{b,\mathrm{av}}^{(1)} \right) h_1, \tag{81}$$

where the derivative of $\overline{\tau}_b^{(0)}$ is evaluated (at $h = h_0$) by means of the analytic result (11), and $\overline{\tau}_{b,\mathrm{av}}^{(1)}$ is given by Eq. (72), again evaluated at $h = h_0$. The corresponding saturated flux is $\overline{q}_{\mathrm{sat}} = q_0 + \epsilon q_{\mathrm{sat},1} \mathrm{e}^{\mathrm{i}k(z-ct)}$ with

$$q_{\mathrm{sat},1} = \frac{\partial \overline{q}_{\mathrm{sat}}}{\partial \tau_b} \tau_1 + \mathrm{i}k h_1 \frac{\partial \overline{q}_{\mathrm{sat}}}{\partial h'}, \tag{82}$$

where the last term accounts for the effect of gravity for non-zero slope. The actual sand flux is $\overline{q} = q_0 + \epsilon q_1 \mathrm{e}^{\mathrm{i}k(z-ct)}$, with, from (74),

$$q_1 = \frac{q_{\mathrm{sat},1}}{1 + \mathrm{i}k L_{\mathrm{sat}}}. \tag{83}$$

Finally, the particle conservation Eq. (73) gives the dimensionless complex wave velocity

$$c = \frac{q_1}{h_1} - q_0 \frac{\cot \delta_w}{\sin \delta_w}. \tag{84}$$

With the above relations, and the derivatives of $\overline{q}_{\mathrm{sat}}$ evaluated from (76), we obtain

$$\frac{c}{q_{\mathrm{ref}}/\tau_{\mathrm{ref}}} = \frac{2\tau_0/\tau_{\mathrm{ref}} - \theta_{t0}}{1 + \mathrm{i}k L_{\mathrm{sat}}} \frac{\tau_1}{h_1} - \frac{\mathrm{i}k \theta_{t0} \cot \chi}{1 + \mathrm{i}k L_{\mathrm{sat}}} \tau_0 - \frac{q_0}{q_{\mathrm{ref}}/\tau_{\mathrm{ref}}} \frac{\cot \delta_w}{\sin \delta_w}, \tag{85}$$

where by (77)

$$\frac{q_{\mathrm{ref}}}{\tau_{\mathrm{ref}}} = \frac{c_q \pi}{108(1-\phi)} \left(\frac{d}{R} \right)^2 \ll 1, \tag{86}$$

which is small since the particle diameter d is small compared to the pipe radius R.

The real part c_{r} of c is the wave velocity (scaled by the velocity $W = Q/R^2$), whereas kc_{i} is the growth rate (scaled by the time R/W). Fig. 15 displays c_{r} and kc_{i} versus wavenumber, for $L_{\mathrm{sat}} = 0$ and the dimensionless parameters given in the figure caption. These numbers correspond, for example, to a pipe of radius $R = 0.02$ m, with oil flow ($W = Q/R^2 = 0.1$ m/s, $\rho = 10^3$ kg/m^3, $\mu = 0.1$ Pa s) over sand grains ($d = 0.2$ mm, $\rho_{\mathrm{p}} = 2600$ kg/m^3, $c_q = 0.85$). In the absence of the stabilizing effects of gravity ($\cot \chi = 0$, dashed curves), the wave velocity is constant (Fig. 15a), whereas the growth rate kc_i is positive for all wavenumbers and increases quadratically with k (Fig. 15b). (If higher order terms were included in the long wavelength expansion, the growth rate would eventually decrease and become negative for high wavenumbers (Charru, 2006).) At any given flow rate, the growth rate kc_i is higher for $h = 1$ (curves with squares) than for $h = 0.5$ (curves with circles), as expected. Including the effect of gravity ($\cot \chi = 2.1$, solid lines) has no effect on the wave velocity, while its diffusive effect (which scales as k^2) simply changes the curvature of the curve showing the growth rate. For $h = 0.5$ (curve with the square), gravity stabilizes all wavenumbers, whereas for $h = 1$ (curve with the circle), it merely decreases the growth rate.

Fig. 16 displays the effect of L_{sat}, for $h = 0.5$ and $\cot \chi = 0$ (no gravity stabilization) and with other parameters as in Fig. 15. The wave velocity (Fig. 16a) appears to be weakly affected by L_{sat}. The growth rate (Fig. 16b) is more sensitive: for $L_{\mathrm{sat}} = 0$ (dashed curve), it is as in Fig. 15; for $L_{\mathrm{sat}} = 0.085$, it is reduced but remains positive (solid line); a relaxation length five times larger (i.e., $L_{\mathrm{sat}} = 0.425$) stabilizes all wavenumbers (dashed-dotted line). These results can be understood from Eq. (85) which gives, still for

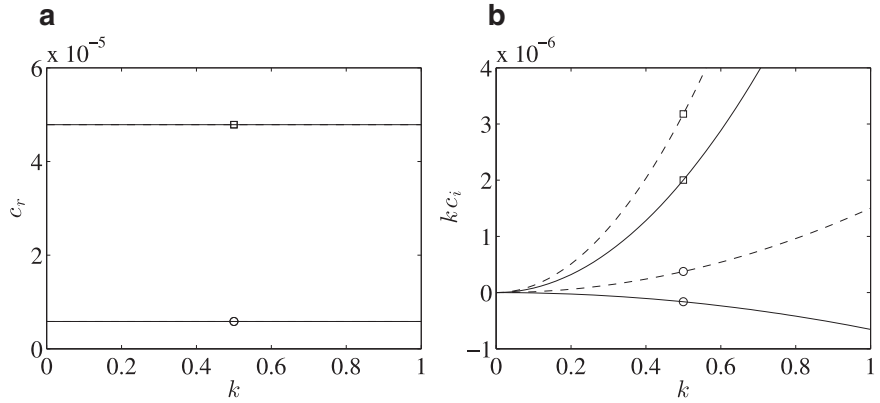

Fig. 15. (a) Wave velocity scaled by Q/R^2, and (b) growth rate scaled by Q/R^3, for $h = 0.5$ (○) and $h = 1$ (□). - - -, $\cot\chi = 0$ (no gravity effect); —-, $\cot\chi = 2.1$. Dimensionless parameters: $h = 0.5$, $\mathrm{Re} = 20$, $q_{\mathrm{ref}} = 2.7 \times 10^{-5}$, $\theta_{t0} = 0.12$ and $L_{\mathrm{sat}} = 0$. The Shields number is $\tau_0/\tau_{\mathrm{ref}} = 0.31$ for $h = 0.5$, and $\tau_0/\tau_{\mathrm{ref}} = 0.68$ for $h = 1$.

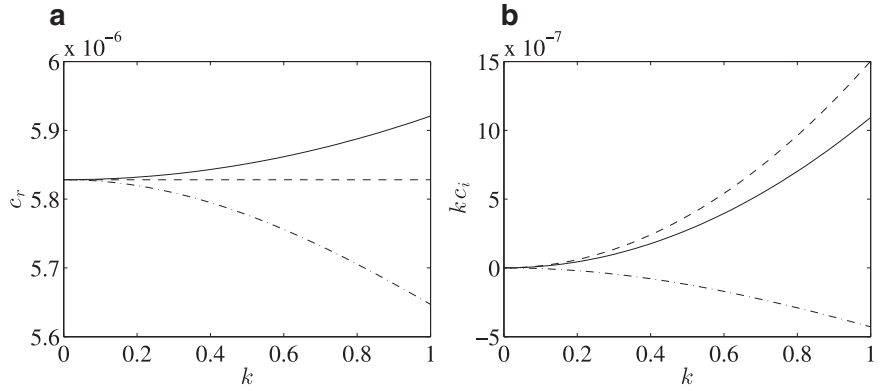

Fig. 16. (a) Wave velocity scaled by Q/R^2, and (b) growth rate scaled by Q/R^3, for $L_{\mathrm{sat}} = 0$ (dashed line), $L_{\mathrm{sat}} = 0.085$ (solid line) and $L_{\mathrm{sat}} = 5 \times 0.085$ (dashed-dotted line). Parameters as in Fig. 15, with $h = 0.5$ and $\cot\chi = 0$ (no gravity effect).

$\cot\chi = 0$,

$$\frac{kc_i}{q_{\mathrm{ref}}/\tau_{\mathrm{ref}}} = \frac{2\tau_0/\tau_{\mathrm{ref}} - \theta_{t0}}{1 + (kL_{\mathrm{sat}})^2}\left(k^2 \mathrm{Re}\,\overline{\tau}^{(1)}_{b,\mathrm{av}} - k^2 L_{\mathrm{sat}}\left.\frac{\partial \overline{\tau}^{(0)}_b}{\partial h}\right|_Q\right). \tag{87}$$

The growth rate is the sum of two terms: a positive part proportional to $\mathrm{Re}\,\overline{\tau}^{(1)}_{b,\mathrm{av}}$, arising from fluid inertia, and a negative part proportional to L_{sat} arising from the relaxation effect. Both terms increase monotonically with wavenumber, with the same functional dependence. Hence, L_{sat} does not provide any cutoff wavenumber. Such a cutoff would arise with the next order included in the long wave expansion, which would weaken the quadratic increase of the inertial term, as mentioned above.

We have checked that use of the exact first-order bed shear stress computed numerically in Section 3, rather than the analytical approximation (72), does not change the velocity and growth rate: the curves in Fig. 16 are indistinguishable.

Finally, some comparison with experimental results is appropriate here. Let us return to the case of zero gravitational and relaxation effects ($\cot\chi = 0$, $L_{\mathrm{sat}} = 0$). The growth rate predicted by (85) then reduces to

$$\frac{kc_{\mathrm{i}}}{q_{\mathrm{ref}}/\tau_{\mathrm{ref}}} = k^2 \mathrm{Re}\,(2\tau_0/\tau_{\mathrm{ref}} - \theta_{t0})\,\overline{\tau}^{(1)}_{b,\mathrm{av}}. \tag{88}$$

Since $\overline{\tau}^{(1)}_{b,\mathrm{av}} > 0$ (see Fig. 14), Eq. (88) shows that the bed is unstable as soon as the stress $\tau_0 = \tau_{t0} = \tau_{\mathrm{ref}}\theta_{t0}$ and particles begin to move. At this threshold the pressure gradient is $\tau_{t0}[(-\partial p^{(0)}/\partial z)/\tau_0]$, where the ratio of the pressure gradient to bed stress is, by (11),

$$\frac{-\partial p^{(0)}/\partial z}{\tau_0} = \frac{2\delta_w}{\sin\delta_w - \delta_w\cos\delta_w}, \tag{89}$$

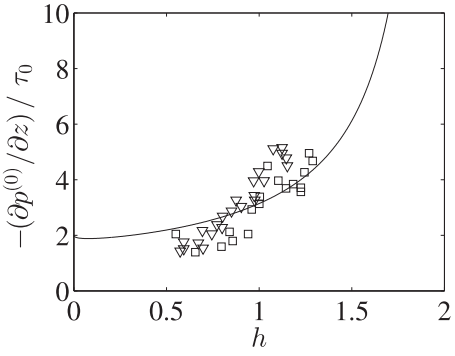

Fig. 17. Ratio (89) of the pressure gradient $-\partial p^{(0)}/\partial z$ and the average bed stress τ_0 on the flat bed, against bed depth h. Squares □ and triangles ▽ represent scaled data from Figs. 5 and 6 of Takahashi and Masuyama (1991).

shown in Fig. 17. For any given sand (i.e., fixed τ_{t0}), the curve in Fig. 17 shows (to within the constant of proportionality τ_{t0}) the pressure gradient required to create motion of the bed of sand, as a function of the bed depth h. Also shown in Fig. 17 are scaled experimental data for the pressure gradient at which the bed becomes unstable, taken from Figs. 5 and 6 of Takahashi and Masuyama (1991). The data correspond to particles of crushed rock (diameter 2.18 mm and specific density 2.74) in pipes of diameter $2R = 49.7$ mm (squares) and $2R = 39.7$ mm (triangles). Assuming a Shields parameter 0.066, we multiply the measured hydraulic gradients by factors of 100 and 80, respectively, to obtain the non-dimensional data in Fig. 17. Although both experimental

and theoretical critical pressure gradients increase with bed depth h, the experimental values increase somewhat more rapidly: we have no explanation for this. We may re-write (89) to give the dimensional pressure gradient required for particles to move (and the bed to be unstable) when the bed stress is $\tau_0 = \tau_{\rm ref}\theta_{t0}$:

$$-\frac{\partial p^{(0)}}{\partial z}\left(\frac{\eta Q}{R^4}\right) = \frac{2\delta_w}{\sin\delta_w - \delta_w\cos\delta_w}\frac{(\rho_{\rm p}-\rho)gd}{R}\theta_t \tag{90}$$

where θ_t is the Shields parameter (41).

Including the effects of gravity and bedload relaxation ($\cot\chi \neq 0$, $L_{\rm sat} \neq 0$) would make little qualitative change to the above results (although the critical Shields number for instability might now be larger than θ_{t0}). Any attempt to make a more detailed comparison between theory and experiment would strongly depend on the choice of the saturation length, which controls the most amplified wavenumber and is still known only poorly (Charru et al., 2013).

7. Summary and conclusions

We have extended existing analytic results for flow over a uniform sand bed, in order to predict the flow corrections that occur when the height of the sand bed is no longer uniform along the length of the pipe, namely: (i) the Stokes secondary flow in the cross-section and (ii) the inertial longitudinal flow. (Note that secondary flows do not occur for laminar plane flow above a uniform sand bed.) In particular, the inertial correction to the stress depends not only on the height h of the sand bed, but also on the bed slope h'. As a result, the stresses acting on a bed perturbation of the form $h \propto \sin(kz)$ need not be in phase with h, and bed instabilities can occur. A noteable result, useful for practical purposes, is that the relative contributions of the mean inertial stress over the bed and over the wall to the total inertial force on the fluid can be accurately estimated from the leading-order, parallel flow calculations.

Various restrictions have been noted in the course of the analysis. The unperturbed flow above the unperturbed, uniform sand bed must be laminar, which requires the Reynolds number $\rho Q/(R\eta)$ (19) to be below the threshold for turbulence. The non-circular form of the fluid cross-section suggests that this criterion should be based on the hydraulic diameter and thus the lengthscale R in the Reynolds number should be replaced by the wetted perimeter $C_b + C_w$ (2). The restriction that the perturbed flow should be laminar requires only $h'{\rm Re} \ll 1$, where the bed slope h', typically $O(d/R)$, can be considered arbitrarily small in a stability analysis. This condition is therefore automatically satisfied when studying the onset of instability. Finally, we have assumed that the stress on the surface of the bed is such that there is a thin bedload layer of moving particles, rather than a completely static bed or a thick layer of suspended particles. This marks the changeover between a static bed and the moving bed that we have shown to be unstable, and occurs at the pressure gradient given by (90).

The area-averaged model of Luchini and Charru (2010a), combined with the approximation for the distribution of stress perturbations over the pipe wall and sand bed, leads rapidly to predictions of the average stress perturbation on the sand bed, without the need for the full analysis of Section 3. Although these area-averaged predictions require only knowledge of the leading-order parallel flow solution for the fluid flow, they are valid up to first-order in the small-slope parameter. The predicted perturbations of the pressure gradient and bed stress are very close to those computed from the full perturbation equations.

The averaged equations, which include the kinetic-energy equation as well as the equations of continuity and momentum, form a closed set of consistent 1D equations which should be useful for predicting sand motion in long pipes, e.g., in the petroleum industry. In particular, they provide a rapid route for predicting the growth of instabilities of the sand bed. The results may equally well be applied to other problems that depend upon the shear rate at the bed/liquid interface, e.g., heat transfer. Since the dynamics of the sand bed are slow, the bed has been assumed quasi-static, but as long as the rate of growth of instabilities is small, there is no reason why the bed cannot be replaced by viscous fluid, thereby enabling an investigation of the rate of growth of instabilities on a fluid/fluid interface.

Acknowledgements

LG was funded by SAIPEM. JDS thanks the IMFT for hospitality during the Michaelmas term 2013, funded by the CNRS.

Appendix A. Flow over a uniform sand bed

A.1. The axial velocity

Stratified flow of two fluids in a pipe has been well studied (Bentwich, 1964; Ranger and Davis, 1979; Brauner et al., 1996; Biberg and Halvorsen, 2000). We follow the presentation of Biberg and Halvorsen (2000), with slightly different notation, since here we consider solid (at rest) and liquid, whereas Biberg and Halvorsen (2000) were interested in the flow of liquid and gas.

We use a bipolar coordinate system (ξ, ζ), as described by Biberg and Halvorsen (2000), with

$$x = \frac{R\sin\delta_b\sinh\xi}{\cosh\xi+\cos\zeta}, \quad y = \frac{R\sin\delta_b\sin\zeta}{\cosh\xi+\cos\zeta}. \tag{91}$$

Note that this is not the standard definition used by others. The surface $\zeta = 0$ corresponds to the sand/liquid interface, $\zeta = \delta_w$ corresponds to the wetted wall of the pipe, and $\zeta = -\delta_b < 0$ corresponds to the portion of the pipe wall in contact with the sand bed. The scale factors for this coordinate system are

$$h_\zeta = h_\xi = \frac{R\sin\delta_w}{\cosh\xi+\cos\zeta} \tag{92}$$

and the Jacobian is

$$J = \frac{\partial(x,y)}{\partial(\xi,\zeta)} = \frac{R^2\sin^2\delta_w}{(\cosh\xi+\cos\zeta)^2}. \tag{93}$$

To find the liquid velocity we need to solve the Poisson Eq. (5). A particular solution of (5) is

$$w^p = \frac{G}{4\eta}(R^2-r^2) = \frac{GR^2\sin\delta_b\sin(\delta_w-\zeta)}{2\eta(\cosh\xi+\cos\zeta)}, \tag{94}$$

which corresponds to Poiseuille flow along a pipe in the absence of any sand bed. This velocity field (94) satisfies the no-slip boundary condition on the pipe wall $\zeta = \delta_w$, but not on the surface of the sand, $\zeta = 0$. To remedy this, we seek a solution $w = w^h$ of the homogeneous equation $\nabla^2 w^h = 0$, with values on the boundary such that $w^p + w^h$ satisfies both the governing Eq. (5) and the no-slip boundary conditions.

In the bipolar coordinate system, w^h satisfies the Laplace equation

$$\frac{\partial^2 w^h}{\partial\xi^2} + \frac{\partial^2 w^h}{\partial\zeta^2} = 0, \tag{95}$$

and the no-slip condition on the pipe wall becomes

$$w^h = 0 \quad \text{on } \zeta = \delta_w. \tag{96}$$

In order that $w^p + w^h$ satisfies the no-slip condition on the

interface $\zeta = 0$, we require

$$w^h = -\frac{GR^2 \sin^2 \delta_w}{2\eta(1+\cosh\xi)} = -\frac{GR^2 \sin^2 \delta_w}{4\eta \cosh^2(\xi/2)} \qquad \text{on } \zeta = 0. \tag{97}$$

We now take Fourier cosine transforms, using

$$\tilde{f}(\omega) = \frac{2}{\pi}\int_0^\infty f(\xi)\cos\omega\xi \,\mathrm{d}\xi, \tag{98a}$$

$$f(\xi) = \int_0^\infty \tilde{f}(\omega)\cos\omega\xi \,\mathrm{d}\omega. \tag{98b}$$

The Fourier transform of the Laplace Eq. (95) gives

$$\frac{\partial^2 \tilde{w}^h}{\partial \zeta^2} - \omega^2 \tilde{w}_h = 0. \tag{99}$$

The boundary condition (96) on the pipe wall becomes

$$\tilde{w}^h = 0 \quad \text{on } \zeta = \delta_w, \tag{100}$$

and the boundary condition (97) on the sand bed transforms to

$$\tilde{w}^h = -\frac{GR^2 \sin^2 \delta_w}{\eta}\left(\frac{\omega}{\sinh\omega\pi}\right) \qquad \text{on } \zeta = 0, \tag{101}$$

where we have used the relation

$$\frac{2}{\pi}\int_0^\infty \mathrm{sech}^2(\xi/2)\cos\omega\xi \,\mathrm{d}\xi = \frac{\omega}{\sinh\omega\pi}. \tag{102}$$

Solutions of the transformed Laplace Eq. (99) that satisfy the no-slip boundary condition (100) on the pipe wall take the form

$$\tilde{w}^h = -\frac{GR^2 \sin^2 \delta_w}{\eta}\frac{\omega\sinh[\omega(\delta_w-\zeta)]}{\sinh\omega\delta_w \sinh\omega\pi}. \tag{103}$$

Taking the inverse transform (98b) of (103), and combining with the particular solution w^p (94), of (5), we find

$$w = w^p + w^h = \frac{GR^2 \sin\delta_w \sin(\delta_w-\zeta)}{2\eta(\cosh\xi+\cos\zeta)} - \frac{GR^2\sin^2\delta_w}{\eta} \times \int_0^\infty \left(\frac{\omega\sinh[\omega(\delta_w-\zeta)]}{\sinh\omega\delta_w\sinh\omega\pi}\right)\cos\omega\xi \,\mathrm{d}\omega. \tag{104}$$

A.2. The volumetric flow rate

Ranger and Davis (1979) evaluate the volumetric flow rate Q in a two-fluid system, and so here we merely indicate how the analysis proceeds when the bed of sand is at rest.

The expression (104) for the liquid velocity w consists of two terms. The first, w^p, is simply Poiseuille flow through a pipe of radius R, and the corresponding contribution to the flow rate can be obtained by integration using polar coordinates (r, ψ). If $\delta_w < \pi/2$, we define $r_1 = R\cos\delta_w/\cos\psi$ and determine the volumetric flow rate

$$Q^p = \frac{G}{2\eta}\int_0^{\delta_w}\mathrm{d}\psi\int_{r_1}^R (R^2-r^2)r\,\mathrm{d}r = \frac{GR^4}{8\eta}\left[\delta_w + \frac{\sin 4\delta_w}{12} - \frac{2}{3}\sin 2\delta_w\right]. \tag{105}$$

If $\delta_w > \pi/2$, we perform this same integration over the region occupied by the sand. The integral over the entire circular cross-section is $G\pi R^4/(8\eta)$, and so the integral over the region occupied by liquid is

$$\frac{G\pi R^4}{8\eta} - \frac{GR^4}{8\eta}\left[\delta_b + \frac{\sin 4\delta_b}{12} - \frac{2}{3}\sin 2\delta_b\right]. \tag{106}$$

Setting $\delta_b = \pi - \delta_w$, we see that (106) is identically equal to the expression (105) for Q^p, which therefore holds for all δ_w.

We now consider the second term u^h in the expression (104) for w, with a contribution to the volumetric flow rate

$$Q^h = -\frac{GR^2\sin^2\delta_w}{\eta}\int_0^{\delta_w}\mathrm{d}\zeta\int_{-\infty}^{\infty}\frac{R^2\sin^2\delta_w\,\mathrm{d}\xi}{(\cosh\xi+\cos\zeta)^2} \times \int_0^\infty\left(\frac{\omega\sinh[\omega(\delta_w-\zeta)]}{\sinh\omega\delta_w\sinh\omega\pi}\right)\cos\omega\xi\,\mathrm{d}\omega. \tag{107}$$

We note that

$$\frac{1}{\pi}\int_0^\infty \frac{\sin a\cos(x\xi)\,\mathrm{d}\xi}{(\cosh\xi+\cos a)} = \frac{\sinh ax}{\sinh\pi x}, \quad a<\pi. \tag{108}$$

Dividing both sides of (108) by $\sin a$ and differentiating with respect to a, we obtain

$$\frac{1}{\pi}\int_0^\infty \frac{\sin a\cos(x\xi)\,\mathrm{d}\xi}{(\cosh\xi+\cos a)^2} = \frac{x\cosh ax}{\sin a\sinh\pi x} - \frac{\cos a\sinh ax}{\sin^2 a\sinh\pi x}. \tag{109}$$

Straightforward manipulations eventually lead to

$$Q^h = \frac{GR^4\sin^4\delta_w}{\eta}\left[\frac{\cot\delta_w}{6} - I\right], \tag{110}$$

where

$$I = \int_0^\infty \frac{\pi\omega^3\cosh\omega\delta_w\,\mathrm{d}\omega}{\sinh\omega\delta_w\sinh^2\omega\pi}. \tag{111}$$

The total volumetric flow rate is therefore

$$Q = Q^p + Q^h = \frac{GR^4}{\eta}\left[\frac{\delta_w}{8} - \frac{\sin 2\delta_w}{24} - \frac{\sin 4\delta_w}{96} - \sin^4\delta_w I\right] = \frac{GR^4}{\eta}\hat{Q}(\delta_w). \tag{112}$$

The integral I (111) can be evaluated numerically, but it proves useful to have an approximate, analytic expression. If $\delta_w \ll \pi$ (pipe nearly full of sand), the convergence of I is ensured by the exponential term $\sinh^2\omega\pi$ in the denominator. We appeal to Watson's lemma and expand $\coth\omega\delta_w$ as a power series in $\omega\delta_w$. The term by term integration of (111) can be performed using

$$\int_0^\infty \frac{x^{2m}\,\mathrm{d}x}{\sinh^2 ax} = \frac{\pi^{2m}}{a^{2m+1}}|B_{2m}|, \tag{113}$$

where the Bernoulli numbers $B_2 = 1/6$, $B_4 = -1/30$, $B_6 = 1/42$, $B_8 = -1/30$. This gives the asymptotic expansion

$$I \approx I_{\text{small}} = \frac{1}{6\delta_w} + \frac{\delta_w}{90} - \frac{\delta_w}{1890} + \frac{\delta_w}{14175} + \cdots, \quad \delta_w \ll \pi. \tag{114}$$

The relative error $(I_{\text{small}} - I)/I < 0.019$ for $\delta_w < 2.22$, and is only 0.17 even when $\delta_w = \pi$. However, in the expression (112) for Q, I is multiplied by $\sin^4\delta_w$, and makes a negligible contribution to Q in the limit $\delta_w \to \pi$. The estimate Q_{small} obtained using the approximation I_{small} has a relative error $|Q - Q_{\text{small}}|/Q < 0.0034$.

When $\delta_w \ll 1$ the height of the sand bed is $h \approx R\left(2 - \delta_w^2/2 + \cdots\right)$. Expanding (112), and using the expansion (114), we find

$$Q \approx \frac{GR^4}{105\eta}\delta_w^7 \approx \frac{GR^4}{105\eta}2^{7/2}\left(2-\frac{h}{R}\right)^{7/2}, \quad \delta_w \ll 1. \tag{115}$$

However, the case $\delta_b \ll \pi$ when there is only a little sand at the bottom of the pipe is important, and it is desirable to know how the pressure gradient is changed by the presence of a small quantity of sand. We therefore seek an expansion of the integral in

(110) about the limit $\delta_b = \pi - \delta_w \ll 1$, using

$$\coth(\omega\pi - \omega\delta_b) = \coth\omega\pi + \frac{\omega\delta_b}{\sinh^2\omega\pi} + \omega^2\delta_b^2\frac{\cosh\pi\omega}{\sinh^3\pi\omega} + \cdots. \tag{116}$$

We again appeal to Watson's lemma to expand the integrand in (111) and integrate term by term, which leads to the approximation

$$I \approx I_{\text{big}} = \frac{1}{4\pi} + \delta_b\left(\frac{1}{3\pi^2} - \frac{1}{45}\right) + \delta_b^2\left(\frac{5}{12\pi^3} - \frac{1}{36\pi}\right) + \cdots, \quad \delta_b = \pi - \delta_w \ll \pi. \tag{117}$$

In the limit $\delta_b \ll 1$, the depth of the sand bed is $h \approx R\delta_b^2/2$. Expanding (112), and using (117), we find

$$Q \approx \frac{GR^4}{\eta}\left(\frac{\pi}{8} - \frac{\delta_b^3}{6} + \cdots\right) \approx \frac{GR^4}{\eta}\left(\frac{\pi}{8} - \frac{1}{6}\left(\frac{2h}{R}\right)^{3/2} + \cdots\right). \tag{118}$$

The asymptotic expansion I_{big} is only useful for small values of δ_b, with $(I - I_{\text{big}})/I < 0.019$ for $\delta_w > 2.22$.

One might suppose that modern computational power has eliminated the need for simple approximations such as those presented above. Nevertheless, they remain useful, for example when using iterative methods to solve inverse problems in which the bed height h is unknown (Biberg, 1999, 2002). In Section 3 we need the derivative $\mathrm{d}Q/\mathrm{d}h$, and this can be found easily and rapidly, with adequate accuracy, by differentiation of (110) and of the approximation (114).

A.3. Wall shear stress

The shear stresses on the circular wall of the pipe ($\zeta = \delta_w$) and on the flat sand bed ($\zeta = 0$) are discussed by Biberg and Halvorsen (2000). Both of these surfaces are surfaces of constant ζ, so the shear stress is

$$\tau_{\zeta z} = \frac{\eta}{h_\zeta}\frac{\partial u_z}{\partial\zeta} \tag{119}$$

with scale factor h_ζ given by (92). Hence

$$\tau_{\zeta z} = \frac{GR}{2}(\cosh\xi + \cos\zeta)\left[\frac{\sin(\delta_w - \zeta)\sin\zeta}{(\cosh\xi + \cos\zeta)^2} - \frac{\cos(\delta_w - \zeta)}{\cosh\xi + \cos\zeta}\right] + GR\sin\delta_w(\cosh\xi + \cos\zeta) \times \int_0^\infty \left(\frac{\omega^2\cosh[\omega(\delta_w - \zeta)]}{\sinh\omega\delta_w\sinh\omega\pi}\right)\cos\omega\xi\,\mathrm{d}\omega. \tag{120}$$

The total force on the sand bed, $\zeta = 0$, is

$$F_b = 2\int_0^\infty \frac{R\sin\delta_w}{\cosh\xi + \cos\zeta}\,\tau_{\zeta z}\big|_{\zeta=0}\,\mathrm{d}\xi = GR^2\sin^2\delta_w\int_0^\infty \mathrm{d}\xi\int_0^\infty \frac{2\omega^2\cosh\omega\delta_w}{\sinh\omega\delta_w\sinh\omega\pi}\cos\omega\xi\,\mathrm{d}\omega - \frac{GR^2}{2}\int_0^\infty \frac{\sin 2\delta_w\,\mathrm{d}\xi}{\cosh\xi + 1}. \tag{121}$$

To evaluate the first integral in (121), we set $\omega' = 0$ in the inversion rule for Fourier cosine transforms,

$$\tilde f(\omega') = \frac{2}{\pi}\int_0^\infty\int_0^\infty \tilde f(\omega)\cos(\omega'\xi)\cos(\omega\xi)\,\mathrm{d}\omega\,\mathrm{d}\xi, \tag{122}$$

to obtain

$$\int_0^\infty \mathrm{d}\xi\int_0^\infty \frac{\omega^2\cosh\omega\delta_w}{\sinh\omega\delta_w\sinh\omega\pi}\cos\omega\xi\,\mathrm{d}\omega = \frac{1}{2\delta_w}. \tag{123}$$

The total force on the sand bed (121) is therefore

$$F_b = GR^2\left(\frac{\sin^2\delta_w}{\delta_w} - \frac{\sin 2\delta_w}{2}\right) \tag{124}$$

and the mean stress is

$$\overline{\tau}_b = \frac{F_b}{C_b} = \frac{GR}{2\sin\delta_w}\left(\frac{\sin^2\delta_w}{\delta_w} - \frac{\sin 2\delta_w}{2}\right). \tag{125}$$

The total force on the wetted portion of the circular wall is

$$F_w = -2\int_0^\infty \frac{R\sin\delta_w}{\cosh\xi + \cos\zeta}\,\tau_{\zeta z}\big|_{\zeta=\delta_w}\,\mathrm{d}\xi = \int_0^\infty \frac{GR^2\sin\delta_w\,\mathrm{d}\xi}{\cosh\xi + \cos\delta_w} - GR^2\sin^2\delta_w\int_0^\infty \mathrm{d}\xi\int_0^\infty \frac{2\omega^2\cos\omega\xi\,\mathrm{d}\omega}{\sinh\omega\delta_w\sinh\omega\pi}. \tag{126}$$

After again using the inversion result (122), we find that the force on the wall is

$$F_w = GR^2\left(\delta_w - \frac{\sin^2\delta_w}{\delta_w}\right) \tag{127}$$

and the mean stress is

$$\overline{\tau}_w = \frac{F_w}{C_w} = \frac{GR}{2\delta_w}\left(\delta_w - \frac{\sin^2\delta_w}{\delta_w}\right). \tag{128}$$

The total force on the boundary of the liquid is

$$F_b + F_w = GR^2\left(\delta_w - \frac{\sin 2\delta_w}{2}\right) = GA, \tag{129}$$

where A (1) is the cross-sectional area of the liquid-filled portion of the pipe.

When $\delta_w \ll 1$ and the pipe is almost full of sand, we see from (125), (128) and (115) that

$$\overline{\tau}_b \approx \overline{\tau}_w \approx GR\frac{\delta_w^2}{6} \approx \frac{G}{3}(2R - h). \tag{130}$$

A.4. A pipe with no sand

When there is no sand at all, the fluid velocity in the pipe is the Poiseuille parabolic velocity profile (94). The volumetric flow rate is $Q_{\text{ns}} = \pi GR^4/(8\eta)$ and the mean velocity is

$$\overline{w} = \frac{W}{\pi} = \frac{Q_{\text{ns}}}{\pi R^2} = \frac{GR^2}{8\eta}. \tag{131}$$

The mean squared velocity is

$$\overline{w^2} = \frac{\int w^2\,\mathrm{d}S}{A} = \frac{G^2R^4}{48\eta^2}, \tag{132}$$

so that

$$\alpha_{\text{ns}} = \frac{\overline{w^2}}{\overline{w}^2} = \frac{4}{3}. \tag{133}$$

Similarly

$$\overline{w^3} = \frac{\int w^3\,\mathrm{d}S}{A} = \frac{G^3R^6}{2^8\eta^3} \quad\text{and}\quad \beta_{\text{ns}} = \frac{\overline{w^3}}{\overline{w}^3} = 2. \tag{134}$$

A.5. A pipe almost full of sand, $\delta_w \ll \pi$

When $\delta_w \ll 1$, we may approximate the thin space occupied by liquid as a thin slot with local height

$$H = \frac{R}{2}\left[\delta_w^2 - (x/R)^2\right]. \tag{135}$$

The cross-sectional area A (1) of the portion of the pipe filled with liquid is

$$A = R^2\left[\delta_w - \frac{\sin 2\delta_w}{2}\right] \approx \frac{2R^2\delta_w^3}{3}, \quad \delta_w \ll 1. \tag{136}$$

The fluid velocity in a uniform slot of height H is

$$w = \frac{G}{2\eta} y(H-y), \tag{137}$$

with local volumetric flow rate

$$q = \int_{y=0}^{H} w\,\mathrm{d}y = \frac{GH^3}{12\eta}. \tag{138}$$

The total flow of liquid in the thin slot is

$$Q = 2\int_0^{R\delta_w} q(x)\,\mathrm{d}x = 2\int_0^{R\delta_w} \frac{GR^3}{96\eta}\left[\delta_w^2 - (x/R)^2\right]^3 \mathrm{d}x = \frac{GR^4}{105\eta}\delta_w^7, \tag{139}$$

in agreement with the limit (115) found previously. The mean velocity is

$$\overline{w} = \frac{WR^2}{A} = \frac{Q}{A} \approx \frac{GR^2\delta_w^4}{70\eta}. \tag{140}$$

Further straightforward integration leads to

$$\overline{w^2} = \frac{\int w^2 \mathrm{d}S}{A} = \frac{G^2R^4\delta_w^8}{3465\eta^2} \quad \text{and} \quad \alpha = \frac{\overline{w^2}}{\overline{w}^2} = \frac{140}{99}, \tag{141}$$

so that, after scaling by the value α_{ns} (133) for Poiseuille flow in a circular cylinder with no sand,

$$\frac{\alpha}{\alpha_{\mathrm{ns}}} = \frac{35}{33} = 1.0606\ . \tag{142}$$

Similarly

$$\overline{w^3} = \frac{\int w^3 \mathrm{d}S}{A} = \frac{G^3R^6\delta_w^{12}}{150150\eta^3} \quad \text{and} \quad \beta = \frac{\overline{w^3}}{\overline{w}^3} = \frac{980}{429}, \tag{143}$$

so that

$$\frac{\beta}{\beta_{\mathrm{ns}}} = \frac{490}{429} = 1.14219. \tag{144}$$

The first-order inertial pressure gradient perturbation can be obtained from the rate of change of kinetic energy (Luchini and Charru, 2010a):

$$Q\frac{\partial p^{(1\mathrm{i})}}{\partial z} = -\frac{\partial}{\partial z}\left[\frac{\rho}{2}A\overline{w^3}\right] = -\frac{\partial}{\partial z}\left[\frac{735\rho Q^3}{286R^4\delta_w^6}\right] = \frac{\mathrm{d}\delta_w}{\mathrm{d}z}\frac{2205\rho Q^3}{143R^4\delta_w^7} = -h'\frac{2205\rho Q^3}{143R^5\delta_w^8}. \tag{145}$$

Hence

$$\frac{\partial p^{(1\mathrm{i})}}{\partial z} = -\left(\frac{Q\rho}{R\eta}\right)\frac{21Gh'}{143\delta_w} = -\left(\frac{Q\rho}{R\eta}\right)\frac{Gh'}{(2-h/R)^{1/2}}\frac{21}{143\sqrt{2}}. \tag{146}$$

The first-order inertial correction to the momentum balance gives

$$C_b\overline{\tau}_b^{(1)} + C_w\overline{\tau}_w^{(1)} - A\frac{\partial p^{(1\mathrm{i})}}{\partial z} = \frac{\partial}{\partial z}\left[\rho A\overline{w^2}\right]. \tag{147}$$

In the limit $\delta_w \to 0$, the mean inertial stress perturbations on the two sides of the slot become

$$\overline{\tau}_b^{(1)} = \overline{\tau}_w^{(1)} = \frac{\partial p^{(1\mathrm{i})}}{\partial z}\frac{A}{4R\delta_w} + \left(\frac{Q\rho}{R^2\eta}\right)GRh'\frac{\delta_w}{66} = \left(\frac{Q\rho}{R^2\eta}\right)GRh'\frac{4\sqrt{2}}{429}(2-h/R)^{1/2}. \tag{148}$$

The maximum slot height, at $x = 0$, is

$$H_{\max} = 2R - h = R\delta_w^2/2, \tag{149}$$

and the maximum velocity is

$$w_{\max} = \frac{GH_{\max}^2}{8\eta} = \frac{105Q}{32R^2\delta_w^3}. \tag{150}$$

From the scaling (146) for $\partial p^{(1\mathrm{i})}/\partial z$ as $\delta_w \to 0$, we conclude that

$$w^{(1\mathrm{i})} \sim \left(\frac{Q\rho}{R^2\eta}\right)h'\frac{Q}{R^2\delta_w^4}. \tag{151}$$

Thus, as $\delta_w \to 0$, the inertial correction $w^{(1\mathrm{i})}$ increases more rapidly than the maximum value $w_{\max}$ (150) of the unperturbed velocity $w^{(0)}$, and the perturbation expansion (20) eventually fails. Although our Reynolds number (19), based on Q/R^2, is constant, a Reynolds number based on the axial velocity within the sand-filled pipe becomes large as the area A (136) available for flow becomes small.

Appendix B. Assessment of the quasi-static assumption

The stability analysis of Section 6 was performed under the assumption of quasi-static flow, with time appearing only in the boundary condition at the bed. This assumption appears justified *a posteriori* in view of the smallness of the growth rate, of order $10^{-6}W/R$, which means that the time scale of bed variations is 10^6 larger than the hydrodynamic time scale R/W. As a further confirmation, we evaluate here the correction to the complex wave velocity related to the flow unsteadiness.

The perturbation in bed height h_1 (78) grows as $\mathrm{e}^{-\mathrm{i}kct}$, and the velocity of the bed surface is

$$\frac{\partial h}{\partial t} = -\epsilon h_1 \mathrm{i}kc\,\mathrm{e}^{\mathrm{i}k(z-ct)}. \tag{152}$$

There must in consequence be a perturbation Q_1 of the volumetric flow rate of liquid, satisfying

$$\frac{\partial Q_1}{\partial z} = 2\sin\delta_b(1-\phi)\frac{\partial h}{\partial t} = -2\sin\delta_b(1-\phi)\epsilon h_1 \mathrm{i}kc\,\mathrm{e}^{\mathrm{i}k(z-ct)}, \tag{153}$$

where the factor $2\sin\delta_b$ represents the (non-dimensional) width of the sand bed in the x direction, and the factor $(1-\phi)$ takes account of liquid that is trapped in the newly created pores in the growing bed of sand. We integrate (153) to obtain

$$Q_1 = -2\sin\delta_b(1-\phi)\epsilon h_1 c\,\mathrm{e}^{\mathrm{i}k(z-ct)}. \tag{154}$$

Since in laminar flow the mean stress τ_0 is proportional to the flow rate Q, the mean stress is perturbed by this change in flow rate, and becomes

$$\tau_0(1+Q_1). \tag{155}$$

In consequence, an additional term

$$-\frac{2(2\tau_0/\tau_{\mathrm{ref}} - \theta_{t0})}{1+\mathrm{i}kL_{\mathrm{sat}}}\tau_0\sin\delta_b(1-\phi)c. \tag{156}$$

is added to the right-hand side of Eq. (85) for c, and this term is small compared to other terms in (85) when c is small.

References

Al-Lababidi, S., Yan, W., Yeung, H., 2012. Sand transportations and deposition characteristics in multiphase flows in pipelines. J. Energy Resour. Tech. Trans. ASME 134, 34501.

Andreotti, B., Forterre, Y., Pouliquen, O., 2013. Granular Media: Between Fluid and Solid. Cambridge University Press.

Bagnold, R., 1941. The Physics of Blown Sand and Desert Dunes. Methuen, London.

Bagnold, R., 1979. Sediment transport by wind and water. Nordic Hydrol. 10, 309–322.

Bentwich, M., 1964. Two-phase viscous axial flow in a pipe. J. Basic Engng 86, 669–672.
Berger, S.A., Talbot, L., Yao, L.S., 1983. Flow in curved pipes. Ann. Rev. Fluid Mech. 15, 461–512.
Biberg, D., 1999. Liquid wall friction in two-phase turbulent gas laminar liquid stratified pipe flow. Can. J. Chem. Engng 77, 1073–1082.
Biberg, D., 2002. Holdup and pressure drop in two-phase laminar stratified pipe flow. Multiphase Sci. Techol. 14, 267–301.
Biberg, D., Halvorsen, G., 2000. Wall and interfacial shear stress in pressure driven two-phase laminar stratified pipe flow. Int. J. Multiphase Flow 26, 1645–1673.
Brauner, N., Rovinsky, J., Maron, D.M., 1996. Analytical solution for laminar-laminar two-phase stratified flow in circular conduits. Chem. Engng Comm. 141, 103–143.
Charru, F., 2006. Selection of the ripple length on a granular bed sheared by a liquid flow. Phys. Fluids 18, 121508.
Charru, F., Andreotti, B., Claudin, P., 2013. Sand ripples and dunes. Ann. Rev. Fluid Mech. 45, 469–493.
Charru, F., Mouilleron, H., Eiff, O., 2004. Erosion and deposition of particles on a bed sheared by a viscous flow. J. Fluid Mech. 519, 55–80.
Doron, P., Barnea, D., 1995. Pressure drop and limit deposit velocity for solid-liquid flow in pipes. Chem. Eng. Sci. 50, 1595–1604.
Doron, P., Barnea, D., 1996. Flow pattern maps for solid-liquid flow in pipes. Int. J. Multiphase Flow 22, 273–283.
Doron, P., Granica, D., Barnea, D., 1987. Slurry flow in horizontal pipes-experimental and modeling. Int. J. Multiphase Flow 13, 535–547.
Fredsøe, J., 1974. On the development of dunes in erodible channels. J. Fluid Mech. 64, 1–16.
Goharzadeh, A., Rodgers, P., Wang, L., 2013. Experimental characterization of slug flow on solid particle transport in a 1 deg upward inclined pipeline. J. Fluids Eng., Trans. ASME 135, 081304.
Hecht, F., 2012. New development in FreeFEM++. J. Numer. Math. 20, 251–265.
Kuru, W.C., Leighton, D.T., McCready, M.J., 1995. Formation of waves on a horizontal erodible bed of particles. Int. J. Multiphase Flow 21, 1123–1140.
Lin, P.Y., Hanratty, T.J., 1986. Prediction of the initiation of slugs with linear stability theory. Int. J. Multiphase Flow 12, 79–98.
Luchini, P., Charru, F., 2010a. Consistent section-averaged equations of quasi-one-dimensional laminar flow. J. Fluid Mech. 656, 337–341.
Luchini, P., Charru, F., 2010b. The phase lead of shear stress in shallow-water flow over a perturbed bottom. J. Fluid Mech. 656, 516–539.
Manton, M.J., 1971. Low Reynolds number flow in slowly varying axisymmetric tubes. J. Fluid Mech. 49, 451–459.
Oroskar, A.R., Turian, R.M., 1980. Critical velocity in pipeline flow of slurries. AIChE J. 26, 550–558.
Ouriemi, M., Aussillous, P., Guazzelli, E., 2009a. Sediment dynamics. Part 1. Bed-load transport by laminar shearing flows. J. Fluid Mech. 636, 295–319.
Ouriemi, M., Aussillous, P., Guazzelli, E., 2009b. Sediment dynamics. Part 2. Dune formation in pipe flow. J. Fluid Mech. 636, 321–336.
Peker, S.M., Helvacı, Ş.Ş, 2008. Solid–Liquid Two Phase Flow. Elsevier, Amsterdam, the Netherlands.
Peysson, Y., Ouriemi, M., Medale, M., Aussillous, P., Guazzelli, E., 2009. Threshold for sediment erosion in pipe flow. Int. J. Multiphase Flow 35, 597–600.
Ranger, K.B., Davis, A.M.J., 1979. Steady pressure driven 2-phase stratified laminar-flow through a pipe. Can. J. Chem. Engng 57, 688–691.
Salama, M.M., 2000. Sand production management. J. Energy Resour. Tech. 122, 29–33.
Soepyan, F.B., Cremaschi, S., Sarica, C., Subramani, H.J., Kouba, G.E., 2014. Solids transport models comparison and fine-tuning for horizontal, low concentration flow in single-phase carrier fluid. AIChE J. 60, 76–122.
Takahashi, H., Masuyama, T., 1991. Stability criterion for the surface of the deposit bed of solid-liquid flows in horizontal pipes. J. Chem. Eng. Japan 24, 319–325.
Takahashi, H., Masuyama, T., Noda, K., 1989. Unstable flow of a solid-liquid mixture in a horizontal pipe. Int. J. Multiphase Flow 15, 831–841.
Todd, L., 1977. Some comments on steady, laminar flow through twisted pipes. J. Eng. Math. 11, 29–48.
Turian, R.M., Hsu, F.-L., Ma, T.-W., 1987. Estimation of the critical velocity in pipeline flow of slurries. Powder Tech. 51, 35–47.